

# Bulk and Surface Properties of Dipolar Fluids

B. Groh and S. Dietrich

*Fachbereich Physik, Bergische Universität Wuppertal,*

*D-42097 Wuppertal, Federal Republic of Germany*

(February 13, 2018)

## Abstract

Based on density-functional theory we analyze the full phase diagram, the occurrence of long-ranged orientational order, and the structural properties of dipolar fluids. As a model system we consider the Stockmayer fluid that consists of spherical particles interacting via a Lennard-Jones potential plus dipolar forces. For sufficiently strong dipole moments one finds a region where a fluid phase with long-ranged orientational order is stable. For all sample shapes with the exception of a long thin needle this phase exhibits a spatially inhomogeneous magnetization which depends on the actual shape. We determine the details of the magnetization structure in a cubic sample in the absence and in the presence of an external magnetic field. One obtains a vortexlike structure with an escape of the magnetization into the axis direction near the vortex axis and two point defects where the absolute value of the magnetization is strongly reduced. If the spherical cores of the particles are replaced by elongated or oblate shapes a nematic phase without spontaneous magnetization is also possible due to the anisotropic steric interactions. We study the interplay of this nematic ordering with ferromagnetism in fluids of dipolar hard ellipsoids. Orientational order arises locally in the isotropic fluid phases near the liquid-gas interface of the Stockmayer fluid. Density-functional theory allows us to determine density and orientational order profiles as well as the surface tension of this interface.

## I. INTRODUCTION

Spontaneous symmetry breaking induced by phase transitions is one of the central themes of statistical physics. From a homogeneous and isotropic liquid phase transitions can occur to phases with positional or orientational long-ranged order of the individual particles. Here we are mainly interested in the case of pure orientational order. Well known examples of such systems are the nematic liquid crystals. Initially, it was suspected that dipolar interactions are responsible for the formation of the nematic state [1]. Later, it became clear that the short-ranged steric interactions between strongly anisotropic (elongated or disk-like) nonpolar molecules are sufficient to generate a nematic phase. On the other hand, it is an interesting question whether dipolar interactions alone, i.e., in the absence of anisotropic steric interactions, are also capable of stabilizing an orientationally ordered liquid. That this is indeed possible has been shown for the first time some years ago in computer simulations of a dipolar soft sphere fluid by Wei and Patey [2,3]. Similar observations were made for dipolar hard spheres [4–6] and the Stockmayer fluid [7], in which the spherically symmetric Lennard-Jones potential is added to the dipolar interactions. Depending on whether one deals with electric or magnetic dipole moments this new phase, in which the dipoles are aligned over macroscopic distances, is called a ferroelectric or ferromagnetic liquid. In the following we will adopt the magnetic language keeping in mind that all results are equally valid in the electric case. Theoretically this phase transition was predicted within mean-field theory for a dipolar lattice gas [8] and by a generalized van der Waals theory [9]. A density-functional theory using as input direct correlation functions of the isotropic liquid obtained from an integral equation theory qualitatively confirmed these findings [10]. However, more recent work along the same lines [11] predicts that the ferromagnetic liquid is metastable with respect to freezing. It might be possible to improve upon this approach by directly calculating the direct correlation function in the ordered phase using the methods of Ref. [12]. The present authors also developed a density-functional description [19,21] using a relatively crude approximation for the pair correlation function, whose results will be reviewed in this paper. In contrast to Ref. [10] and to the simulations this approach enables one to map out whole phase diagrams which turn out to exhibit an interesting topology varying with the dipole strength. Other authors have focused on the isotropic-ferromagnetic spinodal which corresponds to a divergence of the dielectric constant, whose position can be estimated using correlation functions from different integral equation theories [13,14]. Finally, we mention perturbation theory as an alternative approach to determine successfully liquid-vapor coexistence of Stockmayer fluids with rigid or polarizable dipoles [15–18].

In all theoretical treatments particular care must be taken of the long range of the dipolar interaction [19,20] which may give rise to diverging integrals. Several approaches to handle these problems have been suggested [10,19,20], the most consistent one being an explicit performance of the thermodynamic limit starting from a large but finite sample of a given shape [19]. For a homogeneously magnetized fluid one finds an energy contribution that depends on the sample shape. However, this shape dependence disappears if inhomogeneously magnetized configurations are taken into account [22,21].

These complications do not arise in Heisenberg fluids governed by short-ranged exchange interactions for which similar phase transitions and phase diagrams have been found [23–25]. For this model as well as for the corresponding Ising fluid [28] there is an ongoing discussion

concerning the values of the critical exponents describing the isotropic-ferromagnetic transition [26–28]. A Potts fluid with  $q \geq 3$  states exhibits only first-order isotropic-ferromagnetic transitions [29]. For a review of the properties of dipolar and spin fluids as obtained from simulations see Ref. [24].

Experimentally a ferromagnetic liquid phase in dipolar fluids has not yet been found. The dipole moments of molecular fluids seem to be too low, though only by a small factor, compared to those that led to ferromagnetism in the simulations. In ferrofluids [30], i.e., colloidal suspensions of small single-domain ferromagnetic particles, chemical tailoring facilitates higher reduced dipole moments; the relevant dimensionless quantity is  $k_B T m^2 / \sigma^3$  where  $m$  is the dipole moment and  $\sigma$  the particle diameter. However, in the simulations the phase transition always occurs at high packing fractions that are presently not attainable in ferrofluids. Due to the combination of fluidity and strong paramagnetism ferrofluids already have a wide range of technical applications that would certainly be enlarged if a ferromagnetic phase could be established. Electro-rheological and magneto-rheological fluids [31] also have high technological relevance. In these systems dipole moments are induced in the colloidal particles by external electric or magnetic fields and large differences between the permittivities of the solute and the solvent which then give rise to strong dipolar particle interactions having a pronounced effect on their rheological properties. However, spontaneous orientational order in the absence of external fields is not possible in these fluids.

Ferromagnetic metals become paramagnetic already far below their melting temperature. Therefore it came as a surprise when recently ferromagnetism was detected for the first time in a liquid metal. In  $\text{Co}_{80}\text{Pd}_{20}$  the melting temperature is sufficiently close to the Curie temperature so that ferromagnetism in the liquid state can be reached by undercooling [32–34]. For the formation of the ferromagnetic order in these materials short-ranged exchange interactions play an important role. However, in addition dipolar interactions are also present and, as in solid ferromagnets, are essential in forming the domain structure. Therefore for these systems we expect strong similarities to the behavior of dipolar fluids as discussed here.

Two other closely related peculiarities of simple dipolar fluids have attracted much attention recently. Strongly dipolar hard or soft spheres form chains of head-to-tail aligned particles at very low densities [35,36]. The chain formation hinders the condensation of liquid droplets. Thus a certain amount of spherically symmetric dispersion interaction is necessary in order to obtain liquid-gas coexistence in a dipolar fluid [37] (but see also Ref. [38]). Alternatively, liquid-gas coexistence of hard dipolar particles is promoted if they are slightly elongated, which renders the energies of the head-to-tail and the antiparallel side-to-side configuration more equal. It has been shown that for a narrow regime of aspect ratios a liquid phase condensates [39]. The relation between chaining and condensation has been studied in a number of theoretical papers [40–42,38].

The solid phases of dipolar fluids are less well studied. In simulations a body-centered tetragonal structure, which has also been found experimentally in electrorheological fluids [43], as well as fcc structures with different types of orientational order were examined [5], but it was not possible to sort out the thermodynamically stable phase. Two early density-functional approaches [44,45] did not find a ferromagnetic solid, but both suffer from algebraic errors [46] and an incorrect treatment of the long-ranged dipolar interaction [47]. Our own density-functional results for the freezing of the Stockmayer fluid are presented

in Sec. V. Ferromagnetism in amorphous dipolar solids is discussed in Refs. [48–50].

The ferromagnetic liquid should be more stable in fluids of oblate instead of spherical particles. Indeed a ferromagnetic phase is formed in a fluid of cut spheres while at lower temperatures a columnar phase with ferromagnetic order only within the columns is observed [51]. The relations between nematic and ferromagnetic order in fluids of dipolar hard ellipsoids are discussed in Sec. VI within the framework of a simple density-functional theory.

Once the bulk phases and their coexistence are established one can study the interfacial properties which arise if different phases are brought into spatial contact with each other or with external walls. These cases can, in principle, be analyzed using the same density functionals as for the bulk. This is demonstrated in Sec. VII for the interface between the isotropic gas and the isotropic liquid which exhibits local orientational order. For dipolar hard spheres and Stockmayer fluids other theoretical approaches to this problem can be found in Refs. [52–54]. There is also an extensive literature concerning more realistic models of specific substances such as water or methanol using lattice-gas theory [55,56], integral equation theory [57], density-functional theory [58], and Monte Carlo simulation [59].

Non-planar interfaces arise in liquid drops and clusters. Metastable spherical liquid drops have been studied with density-functional theory by Talanquer and Oxtoby [60,61] in connection with the analysis of liquid nucleation in supersaturated dipolar gases. In computer simulations of small dipolar clusters [62,63] interestingly at low temperatures one finds vortexlike orientational order similar to the bulk structure of the ferromagnetic phase as discussed in Sec. III.

## II. MODEL AND THEORETICAL APPROACH

We study the Stockmayer model of a dipolar fluid. It is defined by the interaction potential

$$w(\mathbf{r}_{12}, \omega, \omega') = w_{LJ}(r_{12}) + w_{dip}(\mathbf{r}_{12}, \omega, \omega') \quad (1)$$

where  $\mathbf{r}_{12} = \mathbf{r} - \mathbf{r}'$  is the interparticle vector and the orientation of the dipole moments is denoted by  $\omega = (\theta, \phi)$ . The Lennard-Jones potential  $w_{LJ}(r) = 4\epsilon[(\sigma/r)^{12} - (\sigma/r)^6]$  with parameters  $\epsilon$  and  $\sigma$  describes the spherically symmetric dispersion interaction as well as the short-ranged repulsion. The dipolar potential due to point dipoles embedded in the center of the particles is given by

$$w_{dip}(\mathbf{r}, \omega, \omega') = -\frac{m^2}{r^3} (3(\hat{\mathbf{m}}(\omega)\hat{\mathbf{r}})(\hat{\mathbf{m}}(\omega')\hat{\mathbf{r}}) - \hat{\mathbf{m}}(\omega)\hat{\mathbf{m}}(\omega')) \quad (2)$$

where carets denote unit vectors and  $m$  is the absolute value of the dipole moment. A natural extension of this model are mixtures of two polar or polarizable species which also are important in a number of technological applications [64,65].

For a start the Stockmayer fluid is treated within the framework of a relatively simple density-functional theory, which can be derived from an exact expression for the density functional using the low-density limit  $\exp(-\beta w)$  for the pair distribution function [66]. (For more sophisticated choices see Ref. [11].) The resulting functional of the one-particle number density  $\hat{\rho}(\mathbf{r}, \omega)$  of particles at point  $\mathbf{r}$  and with orientation  $\omega$  is

$$\begin{aligned}
\Omega[\{\hat{\rho}(\mathbf{r}, \omega)\}, T, \mu] = & \frac{1}{\beta} \int d^3r d\omega \hat{\rho}(\mathbf{r}, \omega) [\ln(4\pi\Lambda^3 \hat{\rho}(\mathbf{r}, \omega)) - 1] + \int d^3r f_{CS}(\rho(\mathbf{r})) \\
& - \frac{1}{2\beta} \int d^3r d^3r' d\omega d\omega' \hat{\rho}(\mathbf{r}, \omega) \hat{\rho}(\mathbf{r}', \omega') \Theta(r_{12} - \sigma) f(\mathbf{r}_{12}, \omega, \omega') \\
& - \mu \int d^3r d\omega \hat{\rho}(\mathbf{r}, \omega).
\end{aligned} \tag{3}$$

Here  $\Lambda$  denotes the thermal de Broglie wavelength,  $\rho(\mathbf{r}) = \int d\omega \hat{\rho}(\mathbf{r}, \omega)$  is the orientationally averaged density profile,  $f = \exp(-\beta w) - 1$  is the Mayer function,  $\beta = 1/(k_B T)$  corresponds to the inverse temperature, and  $\mu$  is the chemical potential. The first term in Eq. (3) corresponds to the ideal gas free energy while the second term represents the excess free energy of the hard sphere reference system in a local density approximation with the Carnahan-Starling free energy density of hard spheres of packing fraction  $\eta = \frac{\pi}{6} \rho d^3$ :

$$\beta f_{CS}(\rho) = \rho \frac{4\eta - 3\eta^3}{(1 - \eta)^3}. \tag{4}$$

The temperature dependent diameter  $d = \int_0^\sigma dr (1 - \exp(-\beta w_{LJ}(r)))$ , as given by Barker and Henderson [67], accounts for the actually soft repulsion. The third term in Eq. (3) describes the contributions to the free energy due to the long-ranged part of the interactions in a mean-fieldlike manner. The equilibrium density distribution for a given thermodynamic state minimizes the above density functional.

For bulk fluid phases the orientationally averaged density  $\rho$  is taken to be constant and the orientational distribution to be axisymmetric, so that with

$$\hat{\rho}(\mathbf{r}, \omega) = \rho(\mathbf{r}) \alpha(\mathbf{r}, \omega), \quad \int d\omega \alpha(\mathbf{r}, \omega) = 1, \tag{5}$$

in general, here one has

$$\hat{\rho}(\mathbf{r}, \omega) = \rho \alpha(\cos \theta) = \frac{\rho}{2\pi} \sum_{l=0}^{\infty} \alpha_l P_l(\cos \theta). \tag{6}$$

In the isotropic phase  $\alpha(\cos \theta) = 1/(4\pi)$ , i.e.,  $\alpha_l = \delta_{l0}/2$ , while in the ferromagnetic phase also the higher expansion coefficients  $\alpha_{l \geq 1}$  take on non-zero values. If one inserts the expansion in Eq. (6) into the density functional and employs a suitable expansion of the Mayer function into rotational invariants of the three spatial angles  $\omega, \omega'$  and  $\omega_{12}$ , one encounters a conditionally convergent integral that is proportional to  $\alpha_1^2$  [19]. This is a consequence of the slow decay of the dipolar potential (and therefore of the Mayer function). The value of this integral for fluid volume  $V \rightarrow \infty$  depends on the shape of the sample adopted for this limiting process. This integral was determined for ellipsoidal shapes of arbitrary aspect ratio  $k$  and shown to be related to the demagnetization factor known from classical magnetostatics. On the other hand it has been shown by general arguments that the free energies and the phase diagrams of dipolar systems in zero field do not depend on the sample shape [22]. This apparent contradiction is reconciled by the observation that the true equilibrium state of the ferromagnetic liquid corresponds to such a shape-dependent inhomogeneous configuration that in the resulting free energy the shape dependence drops out. Using a general spatially

inhomogeneous orientational distribution, within the present theory we have confirmed that the equilibrium free energy indeed does not depend on the sample shape and is the same as that of the homogeneous state in a needle-shaped volume ( $k \rightarrow \infty$ ) [21]. Therefore the phase diagram determined for this special case is valid for all shapes keeping in mind that for a general shape the ferromagnetic phase exhibits a nontrivial spatial structure. Details of this structure are discussed in the next section. We remark that these inhomogeneities are suppressed by the so-called “tin-foil” boundary conditions that are usually applied in computer simulations, i.e., by surrounding the sample with an infinitely permeable material (a perfect conductor in the electric case, respectively). The free “magnetic charges” in the surrounding material cancel the demagnetization field which leads to shape independence also for homogeneous magnetization. In the following we only consider the more realistic open boundary conditions.

The properties of the Stockmayer fluid can be described in terms of the following dimensionless quantities:

$$T^* = k_B T / \epsilon, \quad \rho^* = \rho \sigma^3, \quad m^* = m / \sqrt{\sigma^3 \epsilon}. \quad (7)$$

Figure 1 displays the phase diagrams in the temperature-density plane as obtained from the present theory for three different values of the reduced dipole moment  $m^*$ . At low dipole moments there is a large coexistence region of the isotropic gas and liquid phases and a second-order transition to the ferromagnetic liquid along a line of critical points. This line ends at the coexistence curve in a critical end point. Upon increasing the dipole moment the isotropic-ferromagnetic transition shifts to lower densities and higher temperatures and a tricritical point emerges below which the transition becomes first order. Moreover all three fluid phases coexist at a triple point. At even higher dipole moments the gas-liquid coexistence becomes metastable and is preempted by the isotropic gas - ferromagnetic liquid transition, so that one is left with only two fluid phases. A similar series of phase diagrams has been obtained from a phenomenological theory [9], while in simulations to date neither the order of the transition nor the topology of the phase diagram have been mapped out.

### III. INHOMOGENEOUS MAGNETIZATION

The arguments leading to the proof of the shape independence mentioned above provide also a characterization of the actual inhomogeneous magnetization configuration for a given sample shape. Locally it should exhibit the same orientational distribution that has been determined for the needle shaped sample, but with a spatially varying preferential direction. This variation should correspond to a magnetization field  $\mathbf{M}(\mathbf{r})$  which on the scale of the system size has zero divergence and a vanishing normal component at the surface [21]. However, for a given shape these conditions do not determine  $\mathbf{M}(\mathbf{r})$  uniquely and we are not aware of a systematic method to construct fields consistent with them. Therefore we pursued an alternative approach by computing this field via a quasi-free minimization of the density functional. A cubic discretization lattice with lattice constant  $a$  and lattice vectors  $\mathbf{R}$  is superimposed on a cubic sample which we have chosen as an example. From Eq. (3) one derives the following approximation for the free energy difference  $\Delta F$  between the isotropic and ferromagnetic phases [68]:

$$\beta\Delta F = \rho a^3 \sum_{\mathbf{R}} \sum_{n=1}^{\infty} \frac{(\sqrt{12\pi}M(\mathbf{R}))^{2n}}{(2n-1)2n(2n+1)} + \frac{1}{2}\rho^2 a^6 \sum_{\mathbf{R}, \mathbf{R}'} \sum_{i,j} M_i(\mathbf{R}) w_{ij}(\mathbf{R} - \mathbf{R}') M_j(\mathbf{R}') \quad (8)$$

with the interaction tensor

$$w_{ij}(\mathbf{R}) = \Theta(R - \sigma) \left[ f_{110}(R)\delta_{ij} + f_{112}(R)(\delta_{ij} - 3\hat{R}_i\hat{R}_j) \right]. \quad (9)$$

The functions  $f_{110}$  and  $f_{112}$  are certain expansion coefficients of the Mayer function that are known analytically. To lowest order in  $m^2$  one has  $f_{110} \sim m^6$  and  $f_{112}(r) \sim (1 - e^{-\beta w_{LJ}})m^2/r^3$  so that  $w_{ij}(\mathbf{R} - \mathbf{R}')$  reproduces the dipolar interaction between the points  $\mathbf{R}$  and  $\mathbf{R}'$ . This expression is minimized with respect to the values of  $\mathbf{M}(\mathbf{R})$  at all lattice points using the simulated annealing algorithm [69]. Up to  $N = 24$  points for each spatial dimension are used which amounts to  $3 \times 24^3 = 41472$  variables.

Results for the thermodynamic parameters  $m^* = 1.5$ ,  $T^* = 2.25$ , and  $\rho^* = 0.94$  are shown in Fig. 2. One of the three perpendicular cubic axes is chosen spontaneously as a vortex axis around which the magnetization field circulates. As one can infer from the sections parallel to the vortex axis (i.e., the  $z$  axis) in Figs. 2(b) and (c)  $\mathbf{M}(\mathbf{r})$  lies essentially in the vortex plane except close to the axis where it “escapes” into the third dimension in order to avoid a line singularity. Since the magnetization is approximately parallel at the surface two point defects at the centers of the top and bottom face are inevitable. The absolute value  $M(\mathbf{r})$ , which in contrast to the common assumption in micromagnetic calculations [70] is not fixed at a constant value, is strongly reduced within the cores of the point defects whereas it is approximately constant throughout the rest of the volume with the exception of thin surface layers. At higher temperatures in the vicinity of the phase transition to the isotropic liquid a reduction of  $M(\mathbf{r})$  occurs also along the whole vortex axis.

The structure in Fig. 2 can also be considered to consist of four triangular domains with four broad  $90^\circ$  domain walls along the diagonals. These walls are clearly induced by the cube edges and would probably be absent in a cylindrical sample. We have computed a suitably defined wall thickness  $\delta$  [21] for different sample sizes  $L$ . In Fig. 3 we show the results as function of  $1/L$  up to the largest systems with  $L/\sigma = 12$ . The various points for the same  $L$  correspond to different values of  $N$  and thus give an indication of the error induced by the discretization. The data are consistent with the conjecture  $\delta/L \rightarrow \text{const}$  for  $L \rightarrow \infty$  which would mean that the wall thickness is determined by the system size [71]. This contrasts with the finite wall thickness in solid ferromagnets that is caused by the existence of easy axes induced by the lattice anisotropy. The whole magnetization configuration fulfills, to a good approximation, the scaling relation

$$\mathbf{M}(r/\sigma, L/\sigma) \approx \mathbf{M}^{(0)}(\mathbf{r}/L) \quad (10)$$

when different sizes within the accessible regime are compared. We conjecture that this holds also in the thermodynamic limit.

The average magnetization of the sample  $\langle \mathbf{M} \rangle = V^{-1} \int d^3r \mathbf{M}(\mathbf{r})$  is approximately zero although  $|\mathbf{M}(\mathbf{r})| \neq 0$ . The positive contribution to  $\langle M_z \rangle$  from the “escape” near the vortex axis is compensated by negative contributions from the regions close to the edges. However, a finite value of  $\langle M_z \rangle$  is expected for cylindrical or spherical [72] samples.

#### IV. EXTERNAL FIELD

An external magnetic field tends to rotate all dipoles into the field direction and thus to destroy any inhomogeneity of  $\mathbf{M}(\mathbf{r})$ . Let us first consider sample shapes which induce a planar zero-field structure. As we have seen, this is approximately true for the cube, but most probably also for a torus [73]. We consider the case that the field is applied perpendicularly to the magnetization plane. If one assumes that the angle by which the magnetization is rotated out of plane is the same throughout the sample one can still treat the inhomogeneous problem quasi-analytically [21]. Upon increasing the external field the parallel component of  $\mathbf{M}$  first increases linearly and finally saturates while the perpendicular components decrease and vanish with a square root singularity at a critical field strength  $H_c$  above which the sample is homogeneously magnetized. One can also determine phase diagrams at fixed external fields which now do depend on the sample shape via the demagnetization factor  $D$  [21]. The results for a cubic or spherical sample ( $D = 1/3$ ) with  $m^* = 1.5$  are shown in Fig. 4. The critical line between homogeneous isotropic and inhomogeneous ferromagnetic fluids in zero field turns into a critical line between homogeneously and inhomogeneously magnetized fluids. With increasing field strength this line together with the tricritical point shifts to higher densities and lower temperatures. (Only for a needle-shaped sample ( $D = 0$ ) this line disappears and the tricritical point turns into a second critical point because all phases are homogeneous.) The small shift of the liquid-gas critical temperature is proportional to  $H^2$  for small fields in accordance with the results of perturbation theory [75]. The influence of an external field on the liquid-gas coexistence has also been studied in Refs. [76,7,77].

If the external field is not perpendicular to the magnetization plane, for small fields the structure is still similar to the zero field result. On the other hand, for example in a cube there are six degenerate zero-field solutions. By using the free minimization procedure described in the previous section one can address the question which of them is selected by a small external field parallel to one of the cube axes. It turns out that a slightly perturbed vortex structure with its axis parallel to the field is favored [68]. The further evolution of the structure with increasing field strength takes place as described above. Again the azimuthal magnetization component around the field direction vanishes at a critical field strength  $H_c$ , leaving an almost homogeneously magnetized sample for  $H > H_c$ . A comparison between the structures in zero field and in a finite field below  $H_c$  is given in Figs. 5 and 6. It is interesting to consider the corresponding behavior of  $\mathbf{M}(\mathbf{r})$  for a *spherical* sample which possesses infinitely many equivalent directions. Fredkin and Koehler [74] have performed micromagnetic calculations for solid spherical particles. For low lattice anisotropy they find again a vortex state, but the vortex axis rotates away from the field direction as  $H$  vanishes.

#### V. SOLID PHASES

It is important to obtain an estimate for the position of the freezing transition in the phase diagram in order to know whether the formation of the ferromagnetic liquid is preempted by freezing. In order to get a reasonable description of the solid phase we have chosen a more sophisticated density functional [47]. The hard sphere reference fluid is now treated within the modified weighted density approximation (MWDA) introduced by Denton and Ashcroft [78] which gives very accurate results for the freezing properties of hard spheres.



The perturbative contribution is changed in a way that reproduces the results of Curtin and Ashcroft [79] in the limit of a Lennard-Jones fluid but also includes a contribution from the Mayer function of the dipolar potential as in Eq. (3). The number density is parametrized as

$$\hat{\rho}(\mathbf{r}, \omega) = \rho(\mathbf{r})\alpha(\omega) = \frac{1}{2\pi} \left(\frac{\lambda}{\pi}\right)^{3/2} \sum_{\mathbf{R}} e^{-\lambda(\mathbf{r}-\mathbf{R})^2} \sum_{l=0}^{\infty} \alpha_l P_l(\cos \theta) \quad (11)$$

where  $1/\sqrt{\lambda}$  is the width of the density peaks at the lattice points  $\mathbf{R}$ . The shape dependent contribution to the density functional has been calculated also for a solid structure. For cubic lattices it has been shown to be the same as that of a liquid.

For the considered parameter values ( $m^* \leq 2$ ) the fcc lattice was found to be more stable than the bct (body centered tetragonal) structure observed in simulations [5]. The phase diagrams obtained by this approach (Figs. 7 and 8) comprise five different phases, among them a ferromagnetic solid (fs) magnetized in the (111) direction, and a plastic solid (s) without orientational order. The transition between the liquid phases with and without orientational order extends into the solid region. For dipole moments larger than  $m^* \approx 1$  there is indeed a region with a stable ferromagnetic liquid (fl) phase. However, based on a different density-functional theory Klapp and Forstmann [11] have claimed recently that the latter phase is metastable with respect to the solid for all dipole moments, at variance with the simulation results. Thus even the qualitative features of the Stockmayer fluid phase diagram are not yet finally settled.

## VI. NONSPHERICAL PARTICLES

In fluids consisting of nonspherical particles an orientationally ordered liquid phase may already occur in the absence of dipolar interactions. This nematic phase can be stabilized by short-ranged steric interactions between sufficiently elongated or disklike particles. It has a higher symmetry than a ferromagnetic liquid as particle orientations parallel and antiparallel to the preferential direction have identical probabilities. It is interesting to study the interplay of these two ordering mechanisms in a system of nonspherical dipolar particles. Specifically we have considered hard ellipsoids and hard spherocylinders with a central longitudinal dipole moment [80]. In this case, the reference part of the density functional coincides with the hard core part which is well approximated by the so-called decoupling approximation that amounts to replacing the direct correlation function by that of a hard-sphere fluid scaled by the distance of closest approach for given orientations of the particles and their joining vector. The dipolar interaction is again treated perturbatively within the low-density approximation that yields an expression bilinear in the densities with the Mayer function kernel as in Eq. (3).

The properties of this model are determined by the packing fraction  $\eta$ , the dimensionless ratio  $k_B T \sigma_{\perp}^3 / m^2$ , where  $\sigma_{\perp}$  and  $\sigma_{\parallel}$  are the particle diameters measured perpendicular and parallel to the dipole moment, respectively, and the aspect ratio  $\kappa = \sigma_{\parallel} / \sigma_{\perp}$  of the particles. We find that for elongated particles the isotropic-nematic transition is shifted to lower densities by the dipole moment. This trend is in agreement with earlier results from the

Onsager virial theory [81], integral equation theory [82], and a different version of density-functional theory [83]. The two-phase region widens into gas-nematic coexistence at high dipole moments or low temperatures (Fig. 9). For ellipsoids of aspect ratio  $\kappa \lesssim 2$  (Fig. 10) a ferromagnetic fluid (F) appears at high densities, as well as a reentrant nematic phase at high dipole moments that most probably is an artefact of the theoretical approximations. The ferromagnetic phase is reached from the nematic or isotropic states by continuous (dotted lines) or weakly first-order (solid lines) transitions, depending on the temperature and particle aspect ratio. Similar phase diagrams are found for oblate particles ( $\kappa < 1$ , see Fig. 11). If one compares fluids with aspect ratios  $\kappa$  and  $1/\kappa$  the isotropic-nematic coexistence packing fractions are the same for  $m = 0$  (or  $T \rightarrow \infty$ ) but the ferromagnetic phase becomes stable at much higher values of  $k_B T V_0 / m^2$  ( $V_0$  is the particle volume) for a given packing fraction if  $\kappa < 1$ , because in this case the dipole moments can approach each other closer in the most favorable head-to-tail configuration. For the same reason the ferromagnetic liquid should be easier to attain in fluids of oblate than of spherical particles. For dipolar hard spherocylinders one finds an analogous series of phase diagrams as for elongated ellipsoids [80].

## VII. GAS-LIQUID INTERFACE

Up to this point we were only concerned with bulk properties of dipolar fluids and the influence of sample surfaces. If one allows for the presence of interfaces between coexisting bulk phases various new phenomena arise. By imposing appropriate boundary condition in principle one can examine interfaces between any two phases that can coexist according to the phase diagrams shown in the previous sections. These interfaces can be studied with the same density-functional theories, although the calculations will be much more involved due to the lower symmetry of  $\hat{\rho}(\mathbf{r}, \omega)$ . Here we restrain ourselves to the simplest case, i.e., the interface between the isotropic gas and the isotropic liquid [54,66,84]. For this system the number density depends on the coordinate  $z$  normal to the interface and the local orientational order near the interface is described by the first nontrivial coefficient  $\alpha_2(z)$  in an expansion in terms of Legendre polynomials:

$$\hat{\rho}(\mathbf{r}, \omega) = \hat{\rho}(z, \cos \theta) = \frac{1}{2\pi} \rho(z) \left( \frac{1}{2} + \alpha_2(z) P_2(\cos \theta) + \dots \right). \quad (12)$$

(The higher coefficients  $\alpha_{l>2}(z)$  are very small.) The functions  $\rho(z)$  and  $\alpha_2(z)$  have been calculated numerically by solving the integral equation that results from the stationary condition for the density functional. The density profiles are monotonic and for small reduced dipole moment  $m^*$  they depend only weakly on  $m^*$  for fixed distance  $\tau = 1 - T/T_c$  from the critical temperature  $T_c$  (see Fig. 12). Near the interface the particles are preferentially aligned parallel to the interface ( $\alpha_2(z) < 0$ ) on the liquid side and perpendicular to the interface ( $\alpha_2(z) > 0$ ) on the vapor side (Fig. 13). The amplitude of  $\alpha_2(z)$  increases strongly ( $\sim m^{*4}$ ) with the dipole moment. Near the critical point both the density profile

$$\rho^*(z, \tau \rightarrow 0) = \rho_c^* + A_\rho (m^*) \tau^\beta F_\rho(z/\xi) \quad (13)$$

and the orientational profile

$$\alpha_2(z, \tau \rightarrow 0) = A_{\alpha_2}(m^*)\tau^{\beta+2\nu}F_{\alpha_2}(z/\xi) \quad (14)$$

exhibit a scaling behavior. Here  $\xi$  is the bulk correlation length,  $F_\rho$  and  $F_{\alpha_2}$  are scaling functions, and  $A_\rho$  and  $A_{\alpha_2}$  are nonuniversal amplitudes. Within the density functional approach the critical exponents  $\beta$  and  $\nu$  of the order parameter and of the correlation length take on their mean-field value  $\frac{1}{2}$ . Equation (14) has been used to interpret ellipsometric measurements of the liquid-liquid interface of the critical ionic mixture triethyl-n-hexylammonium triethyl-n-hexylboride dissolved in diphenyl ether [85].

The temperature dependence of the surface tension  $\gamma$ , which can be calculated from these profiles, is shown in Fig. 14. The limiting power law  $\gamma(\tau \rightarrow 0) = \gamma_0\tau^{3/2}$  is valid even quite far away from  $T_c$ . The amplitude  $\gamma_0$  increases with increasing dipole strength. The values of  $\gamma$  are (for  $m^* \leq 2$ ) practically unaltered if the orientational profile  $\alpha_2(z)$  is replaced by  $\alpha_2(z) \equiv 0$ . This means that the main influence of the dipolar interaction on the surface tension is due to the change of the bulk phase diagram and of the number density profile but not due to preferential orientations at the interface. This result has been exploited for obtaining estimates of the surface tension of polar fluids from other, more simple analytical approaches and simulations [86].

## REFERENCES

- [1] M. Born, Sitz. Phys. Math. **25**, 614 (1916); Ann. Phys. **55**, 221 (1918).
- [2] D. Wei and G.N. Patey, Phys. Rev. Lett. **68**, 2043 (1992).
- [3] D. Wei and G.N. Patey, Phys. Rev. A **46**, 7783 (1992).
- [4] J.J. Weis, D. Levesque, and G.J. Zarragoicoechea, Phys. Rev. Lett. **69**, 913 (1992).
- [5] J.J. Weis and D. Levesque, Phys. Rev. E **48**, 3728 (1993).
- [6] M.J. Stevens and G.S. Grest, Phys. Rev. E **51**, 5962 (1995).
- [7] M.J. Stevens and G.S. Grest, Phys. Rev. E **51**, 5976 (1995).
- [8] K. Sano and M. Doi, J. Phys. Soc. Jpn. **52**, 2810 (1983).
- [9] H. Zhang and M. Widom, Phys. Rev. E **49**, R3591 (1994).
- [10] D. Wei, G.N. Patey, and A. Perera, Phys. Rev. E **47**, 506 (1993).
- [11] S. Klapp and F. Forstmann, Europhys. Lett. **38**, 663 (1997).
- [12] H. Zhong and R.G. Petschek, Phys. Rev. E **51**, 2263 (1995).
- [13] J.S. Høye and G. Stell, Mol. Phys. **86**, 707 (1995).
- [14] S. Klapp and F. Forstmann, J. Chem. Phys. **106**, 9742 (1997).
- [15] M.E. van Leeuwen, B. Smit, and E.M. Hendriks, Mol. Phys. **78**, 271 (1993).
- [16] G. Kronome, J. Liszi, and I. Szalai, J. Chem. Soc. Faraday Trans. **93**, 3053 (1997); and references therein.
- [17] I. Szalai, G. Kronome, and T. Lukács, J. Chem. Soc. Faraday Trans. **93**, 3737 (1997).
- [18] C. Kriebel and J. Winkelmann, Mol. Phys. **90**, 297 (1997); and references therein.
- [19] B. Groh and S. Dietrich, Phys. Rev. Lett. **72**, 2422 (1994); *ibid* **74**, 2617 (1995); Phys. Rev. E **50**, 3814 (1994).
- [20] M.A. Osipov, P.I.C. Teixeira, and M.M. Telo da Gama, J. Phys. A. **30**, 1953 (1997).
- [21] B. Groh and S. Dietrich, Phys. Rev. E **53**, 2509 (1996).
- [22] R.B. Griffiths, Phys. Rev. **176**, 655 (1968).
- [23] J.M. Tavares, M.M. Telo da Gama, P.I.C. Teixeira, J.J. Weis, and M.J.P. Nijmeijer, Phys. Rev. E **52**, 1915 (1995).
- [24] M.J.P. Nijmeijer and J.J. Weis, Ann. Rev. Comp. Phys. **IV**, 1 (1996).
- [25] A. Oukouiss and M. Baus, Phys. Rev. E **55**, 7242 (1997).
- [26] M.J.P. Nijmeijer and J.J. Weis, Phys. Rev. Lett. **75**, 2887 (1995).
- [27] M.J.P. Nijmeijer and J.J. Weis, Phys. Rev. E **53**, 591 (1996).
- [28] M.J.P. Nijmeijer, A. Parola, and L. Reatto, Phys. Rev. E **57**, 465 (1998).
- [29] M.A. Załuska-Kotur and Ł.A. Turski, Phys. Rev. A **41**, 3066 (1990).
- [30] R.E. Rosensweig, *Ferrohydrodynamics* (Cambridge University Press, Cambridge, 1985); E. Blums, A. Cebers, and M.M. Maiorov, *Magnetic Fluids* (de Gruyter, Berlin, 1997).
- [31] Proceedings of the 5th International Conference on Electro-Rheological Fluids, Magneto-Rheological Suspensions and Associated Technology, Int. J. Mod. Phys. B **10**, Numbers 23 & 24 (1996).
- [32] D. Platzek, C. Notthoff, D.M. Herlach, G. Jacobs, D. Herlach, and K. Maier, Appl. Phys. Lett. **65**, 1723 (1994).
- [33] J. Reske, D.M. Herlach, F. Keuser, K. Maier, and D. Platzek, Phys. Rev. Lett. **75**, 737 (1995).
- [34] T. Albrecht, C. Bühner, M. Fähnle, K. Maier, D. Platzek, and J. Reske, Appl. Phys. A **65**, 215 (1997).
- [35] J.J. Weis and D. Levesque, Phys. Rev. Lett. **71**, 2729 (1993).

- [36] D. Levesque and J.J. Weis, Phys. Rev. E **49**, 5131 (1994).
- [37] M.E. van Leeuwen and B. Smit, Phys. Rev. Lett. **71**, 3991 (1993).
- [38] J.M. Tavares, M.M. Telo da Gama, and M.A. Osipov, Phys. Rev. E **56**, R6252 (1997).
- [39] S.C. McGrother and G. Jackson, Phys. Rev. Lett. **76**, 4183 (1996).
- [40] R.P. Sear, Phys. Rev. Lett. **76**, 2310 (1996).
- [41] R. van Roij, Phys. Rev. Lett. **76**, 3348 (1996).
- [42] M.A. Osipov, P.I.C. Teixeira, and M.M. Telo da Gama, Phys. Rev. E **54**, 2597 (1996).
- [43] T. Chen, R.N. Zitter, and R. Tao, Phys. Rev. Lett. **68**, 2555 (1992).
- [44] W.E. McMullen and D.W. Oxtoby, J. Chem. Phys. **86**, 4146 (1987).
- [45] S.J. Smithline, S.W. Rick, and A.D.J. Haymet, J. Chem. Phys. **88**, 2004 (1988).
- [46] W.E. McMullen and D.W. Oxtoby, J. Chem. Phys. **88**, 1476 (1988).
- [47] B. Groh and S. Dietrich, Phys. Rev. E **54**, 1687 (1996).
- [48] B.E. Vugmeister and M.D. Glinchuk, Rev. Mod. Phys. **62**, 993 (1990).
- [49] H. Zhang and M. Widom, J. Magn. Magn. Mat. **122**, 119 (1993); Phys. Rev. B **51**, 8951 (1995).
- [50] G. Ayton, M.J.P. Gingras, and G.N. Patey, Phys. Rev. Lett. **75**, 2360 (1995).
- [51] G. Ayton and G.N. Patey, Phys. Rev. Lett. **76**, 239 (1996).
- [52] J. Eggebrecht, K.E. Gubbins, and S.M. Thompson, J. Chem. Phys. **86**, 2286 (1987).
- [53] M. Kasch and F. Forstmann, J. Chem. Phys. **99**, 3037 (1993).
- [54] P.I. Teixeira and M.M. da Gama, J. Phys. Condens. Matter **3**, 111 (1991).
- [55] M. Matsumoto, H. Mizukuchi, and Y. Kataoka, J. Chem. Phys. **98**, 1473 (1993).
- [56] N.A.M. Besseling and J. Lyklema, J. Phys. Chem. **98**, 11610 (1994).
- [57] M.J. Booth, D.-M. Duh, and A.D.J. Haymet, J. Chem. Phys. **101**, 7925 (1994).
- [58] B. Yang, D.E. Sullivan, and C.G. Gray, J. Phys. Condens. Matter **6**, 4823 (1994).
- [59] V.P. Sokhan and D.J. Tildesley, Mol. Phys. **92**, 625 (1997); and references therein.
- [60] V. Talanquer and D.W. Oxtoby, J. Chem. Phys. **99**, 4670 (1993).
- [61] V. Talanquer and D.W. Oxtoby, J. Chem. Phys. **103**, 3686 (1995).
- [62] H.B. Lavender, K.A. Iyer, and S.J. Singer, J. Chem. Phys. **101**, 7856 (1994).
- [63] D. Lu and S.J. Singer, J. Chem. Phys. **103**, 1913 (1995).
- [64] D.J. Henderson and W. Schmickler, J. Chem. Soc. Faraday Trans. **92**, 3839 (1992).
- [65] C. Kriebel and J. Winkelmann, Mol. Phys. **90**, 297 (1997); and references therein.
- [66] P. Frodl and S. Dietrich, Phys. Rev. A **45**, 7330 (1992); Phys. Rev. E **48**, 3203 (1993).
- [67] J.A. Barker and D. Henderson, J. Chem. Phys. **47**, 4714 (1967).
- [68] B. Groh and S. Dietrich, Phys. Rev. Lett. **79**, 749 (1997); Phys. Rev. E, **57**, 4535 (1998).
- [69] W.H. Press, B.P. Flannery, S.A. Teukolsky, and W.T. Vetterling, *Numerical Recipes* (Cambridge University Press, Cambridge, 1989).
- [70] W.F. Brown jr., *Micromagnetics* (Krieger, Huntington, 1978).
- [71] P.G. de Gennes and P.A. Pincus, Solid State Communications **7**, 339 (1969).
- [72] A. Aharoni and J.P. Jakubovics, J. Magn. Magn. Mat. **83**, 451 (1990).
- [73] P.J. Wojtowicz and M. Rayl, Phys. Rev. Lett. **20**, 1489 (1968).
- [74] D.R. Fredkin and T.R. Koehler, IEEE Trans. Magn. **MAG-24**, 2362 (1988); J. Appl. Phys. **67**, 5544 (1990).
- [75] D. Boda, I. Szalai, and J. Liszi, J. Chem. Soc. Faraday Trans. **91**, 889 (1995).
- [76] C.E. Woodward and S. Nordholm, J. Phys. Chem. **92**, 501 (1988).
- [77] D. Boda, J. Winkelmann, J. Liszi, and I. Szalai, Mol. Phys. **87**, 601 (1996).

- [78] A.R. Denton and N.W. Ashcroft, *Phys. Rev. A* **39**, 4701 (1989).
- [79] W.A. Curtin and N.W. Ashcroft, *Phys. Rev. Lett.* **56**, 2775 (1986).
- [80] B. Groh and S. Dietrich, *Phys. Rev. E* **55**, 2892 (1997).
- [81] A.G. Vanakaras and D.J. Photinos, *Mol. Phys.* **85**, 1089 (1995).
- [82] A. Perera and G.N. Patey, *J. Chem. Phys.* **91**, 3045 (1989).
- [83] C. Vega and S. Lago, *J. Chem. Phys.* **100**, 6727 (1994).
- [84] P. Frodl and S. Dietrich, *Phys. Rev. E* **48**, 3741 (1993).
- [85] C.L. Caylor, B.M. Law, P. Senanayake, V.L. Kuzmin, V.P. Romanov, and S. Wiegand, *Phys. Rev. E* **56**, 4441 (1997).
- [86] S. Abbas, P. Ahlström, and S. Nordholm, *Langmuir* **14**, 396 (1998).

## FIGURES

FIG. 1. Phase diagrams of the Stockmayer fluid for three different values of the reduced dipole moment  $m^*$ , including the ferromagnetic liquid phase. The dashed line  $\rho_{fc}(T)$  denotes a line of critical points,  $T_c$  is the gas-liquid critical point, and the shaded areas represent two-phase regions. In part (a) the critical line ends at the coexistence line in a critical end point  $T_{cep}$ , while in (b) and (c) a tricritical point  $T_t$  arises, below which the isotropic-ferromagnetic transition becomes first order. The dotted lines represent the metastable parts of the coexistence curve of the isotropic phases.

FIG. 2. Magnetization structure of a ferromagnetic liquid in a cubic volume with edge length  $L/\sigma = 7.2$ ,  $20^3$  mesh points, and  $T^* = 2.25$ . The three parts of the figure represent sections (a) for fixed  $z = 0.025L$ , (b) fixed  $y = -0.075L$ , and (c) fixed  $y = -0.225L$ ; the origin is at the center of the cube. The arrows represent projections of the local magnetization at their midpoint onto the section plane. The  $z$  axis is the vortex axis. Part (c) demonstrates that in the vicinity of this axis the magnetization “escapes” from the vortex plane.

FIG. 3. The domain wall thickness  $\delta$  in a cubic sample measured within the plane  $z = 0$  at distance  $r = L/2^{3/2}$  from the center, i.e., at half distance between the center and the edges. The different results for the same value  $L^* = L/\sigma$  correspond to different numbers of mesh points used for the minimization. The extrapolation to  $1/L = 0$  suggests a finite value of  $\delta/L$  in the thermodynamic limit.

FIG. 4. Phase diagrams for  $m^* = 1.5$  and various fixed values of the reduced external field strength  $H^* = H\sqrt{\sigma^3/\epsilon}$  for a sample with aspect ratio  $k = 1$  (i.e., demagnetization factor  $D = 1/3$ ). For nonzero fields the inhomogeneous domain structure is partly retained at high densities and low temperatures. The magnetic field shifts the transition line of critical points (dotted curve) and the tricritical point (open circle) towards higher densities and lower temperatures, whereas the gas-liquid critical temperature (full circle) is slightly increased.

FIG. 5. Sections of the magnetization structure orthogonal to the field direction for  $L/\sigma = 9.6$  and  $N = 16$  at  $z/\sigma = -0.9$  (a) without and (b) with an external field  $H^* = H\sqrt{\sigma^3/\epsilon} = 1$  applied in the  $z$  direction. The scale factor which determines the lengths of the arrows is the same in both parts of this figure and also in Fig. 6 below. The transversal components of the magnetization are reduced by the field but the overall feature of the inhomogeneous structure is preserved.

FIG. 6. Vertical sections of the same magnetization structures as in Fig. 5 perpendicular to the  $y$  axis and thus parallel to the field direction for  $y/\sigma = -2.1$ . At this distance of the plane from the center the  $z$  component of the magnetization in zero field is only small, while the external field induces a large  $z$  component everywhere.

FIG. 7. Phase diagram for  $m^* = 1$  including the solid phase as obtained from the generalized density-functional theory. It encompasses five phases: the isotropic gas (g) and liquid (l), the ferromagnetic liquid (fl), the ferromagnetic solid (fs), and the solid without orientational order (s). Two-phase regions are shaded, the dashed lines indicate continuous phase transitions, and the dotted line denotes the triple point. Critical end points are denoted by squares.

FIG. 8. The same as Fig. 7, but for  $m^* = 1.35$ . In addition to the features of Fig. 7 a tricritical point (open circle) and two triple points (dotted lines) occur.

FIG. 9. Phase diagram of hard ellipsoids of revolution with a longitudinal dipole moment and aspect ratio  $\kappa = 3$ .  $\eta$  is the packing fraction. At high temperatures or small dipole moments the transition between the isotropic (I) and the nematic (N) phases is weakly first order, but it widens into a gas-nematic coexistence at low temperatures. Possible smectic and solid phases cannot be described within the present theory.

FIG. 10. The same as Fig. 9 but for aspect ratio  $\kappa = 2$ . Besides the isotropic (I) and nematic (N) phases a ferromagnetically ordered liquid (F) occurs in the intermediate temperature range. The dotted and solid lines denote second- and first-order phase transitions, respectively. The density gap of the I-N transition at  $\eta \simeq 0.68$  cannot be resolved on the present scale. The inset shows that in a narrow temperature range the high temperature continuous N-F transition is turned into a weakly first-order transition generating a tricritical point and an I-N-F triple point. The reentrant nematic phase at low temperatures is probably an artefact of the present theory.

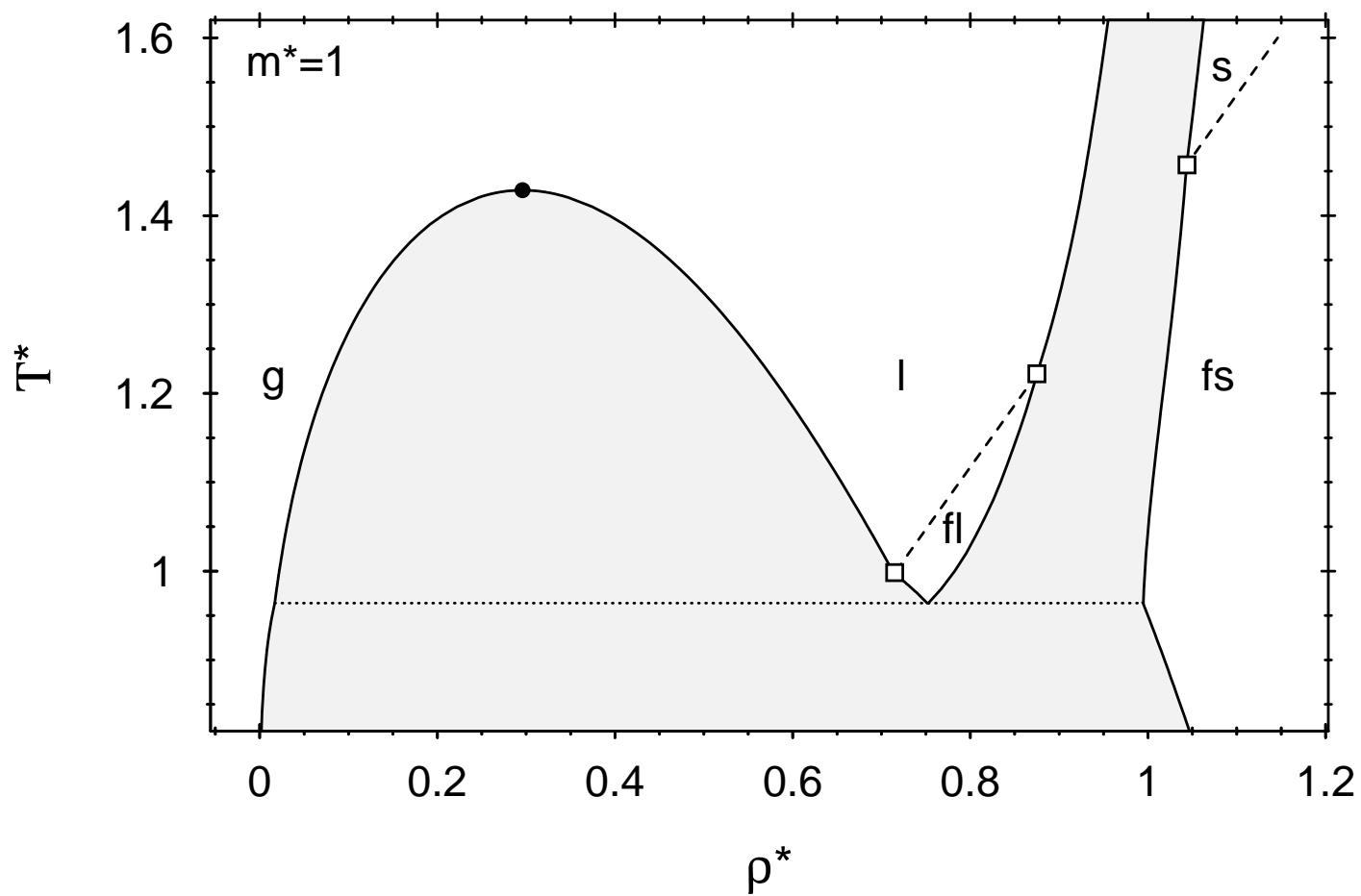
FIG. 11. Phase diagram for oblate ellipsoids with aspect ratio  $\kappa = 1/3$ . The I-N coexistence packing fractions for  $T \rightarrow \infty$  are the same as those for  $\kappa = 3$ , but in contrast to Fig. 9 a ferromagnetic phase is stable at high densities.

FIG. 12. Density profiles for the gas-liquid interface of a Stockmayer fluid for various dipole moments at a fixed reduced temperature  $\tau = 1 - T/T_c = 0.2$ .

FIG. 13. Orientational order profiles  $\alpha_2(z)$  at the gas-liquid interface for the same parameters as in Fig. 12. Note that  $\alpha_2$  is scaled by  $m^{*4}$ . The dipoles are aligned preferentially parallel to the interface on the liquid side and perpendicular to the interface on the gas side. For  $m^* \rightarrow 0$  the profiles approach a limiting form  $\alpha_2(z/\sigma, m^*) = m^{*4} \alpha_2^{(0)}(z/\sigma)$ .

FIG. 14. Temperature dependence of the liquid-gas surface tension  $\gamma_{l,g}^* = \gamma_{l,g} \sigma^2 / \epsilon$  for various dipole moments. The double logarithmic plot in the inset demonstrates that  $\gamma_{l,g} \sim \tau^{3/2}$  for  $\tau \rightarrow 0$ .





*Fig. 7*

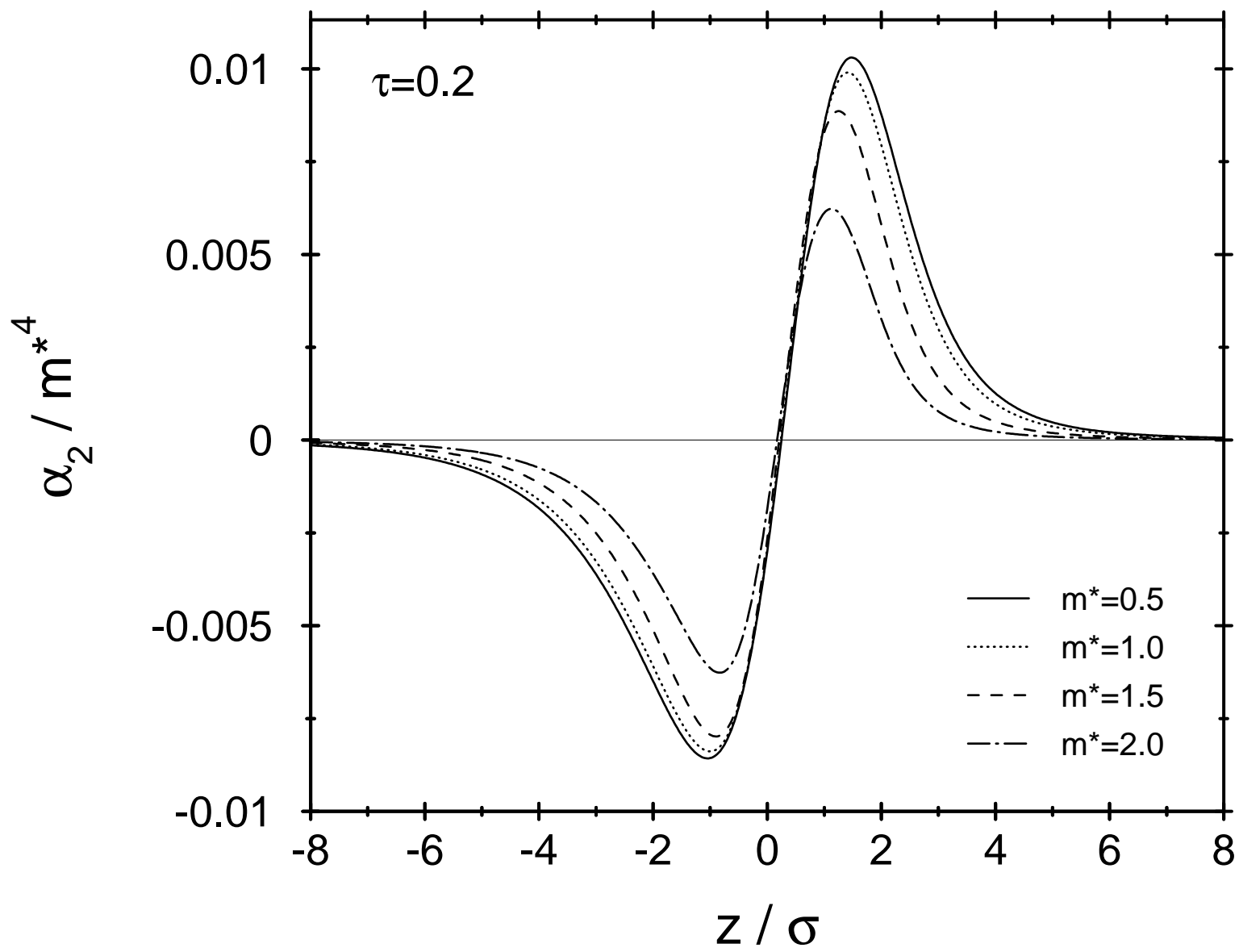
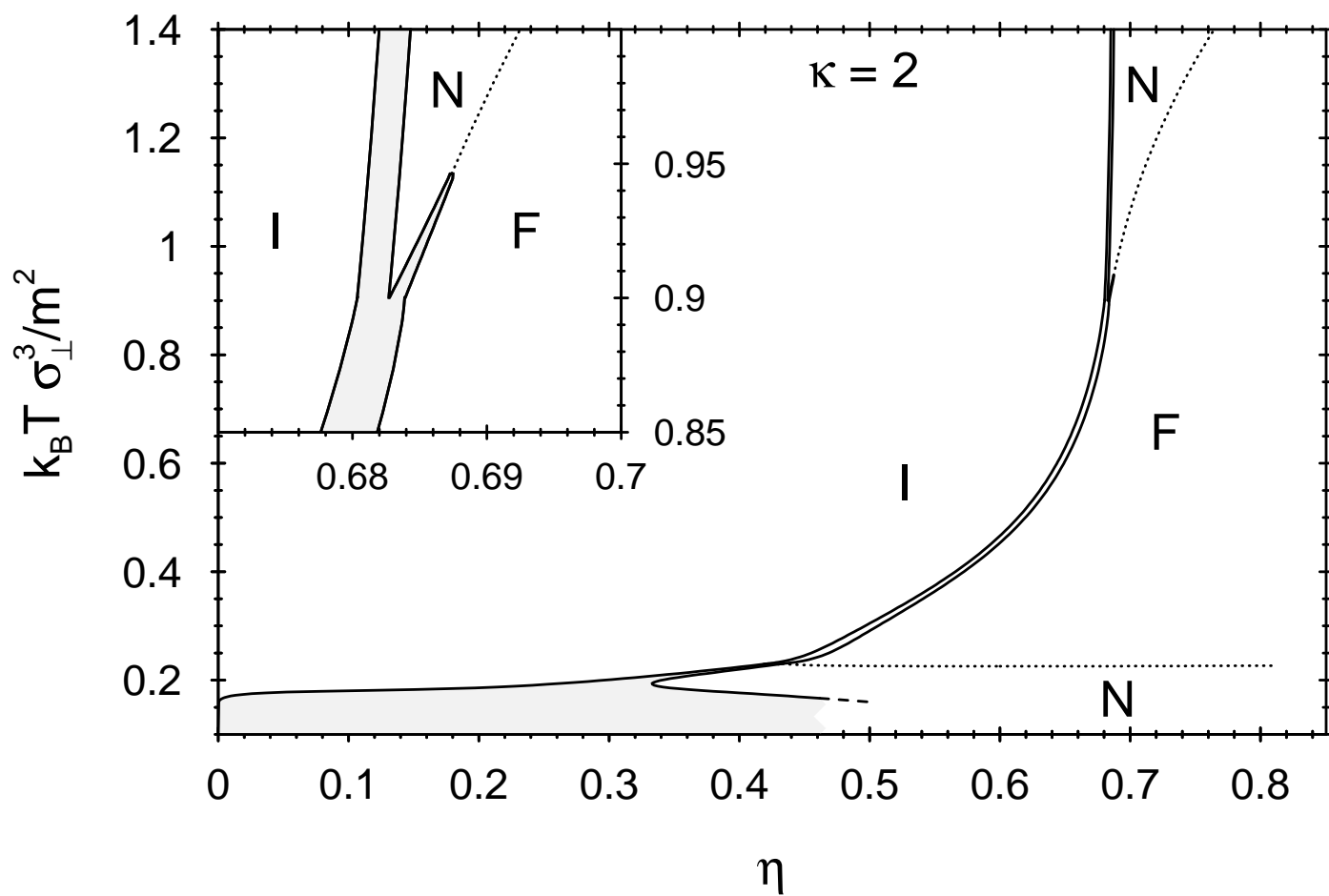
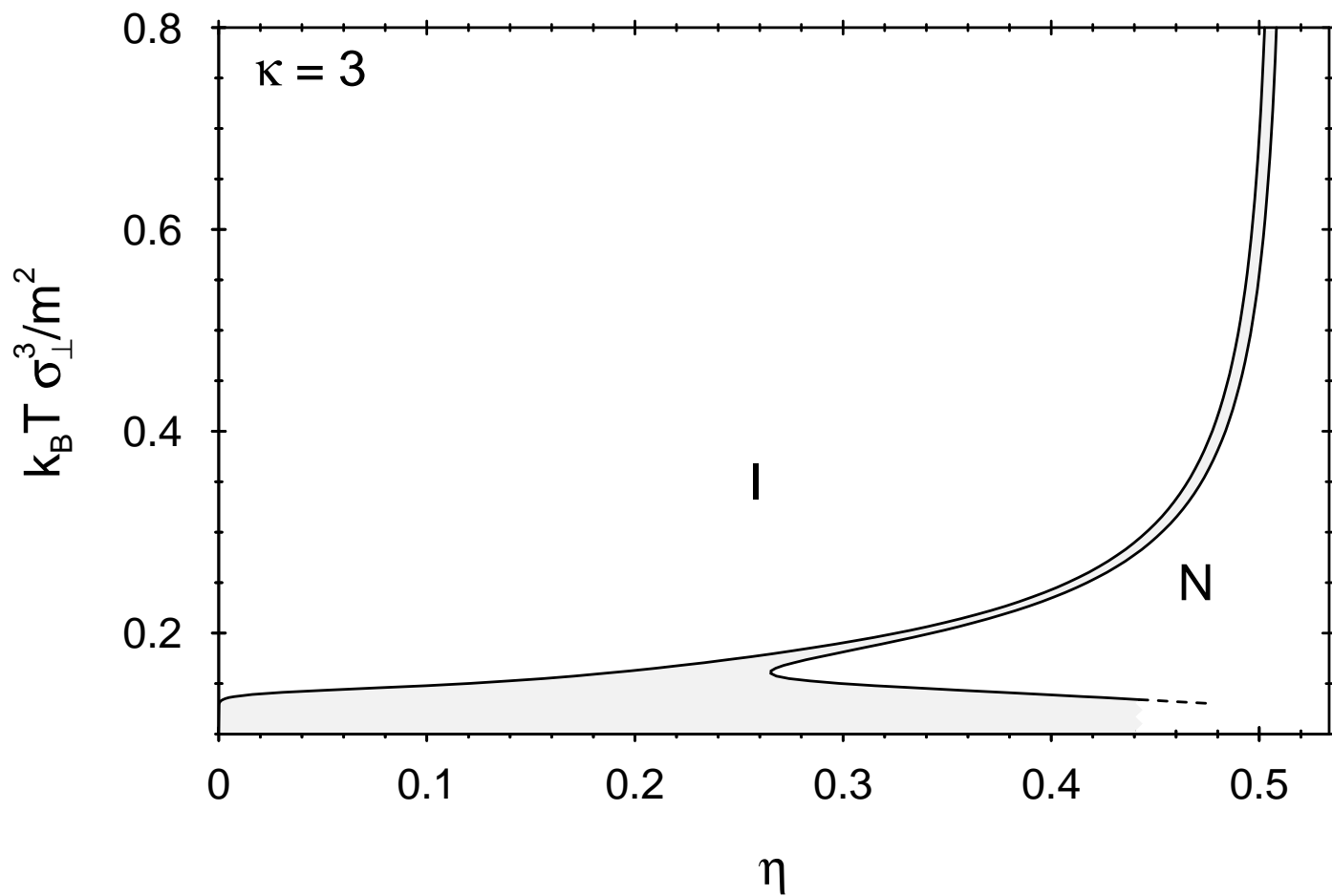


Fig. 13



*Fig. 10*



*Fig. 9*

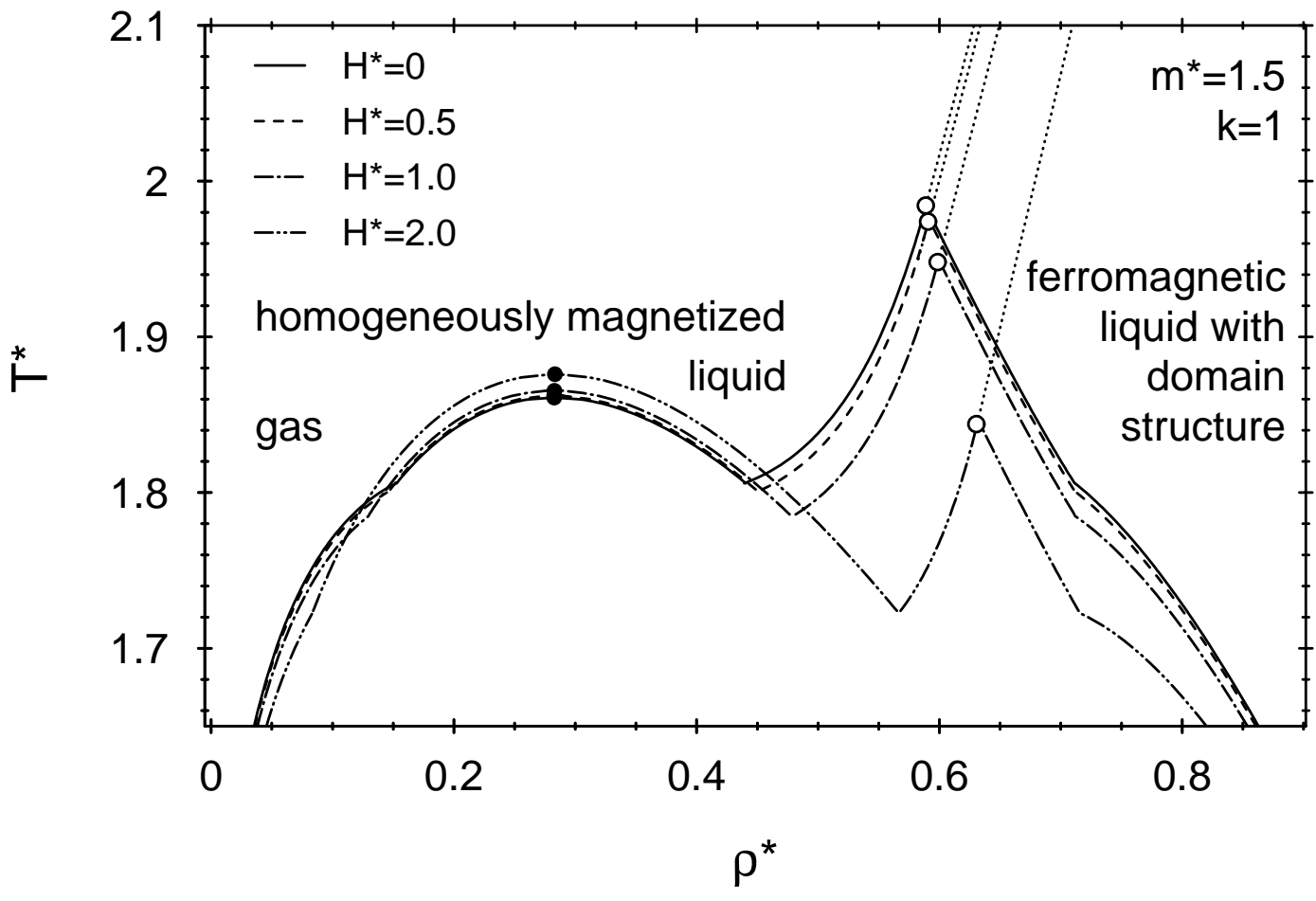


*Fig. 4*

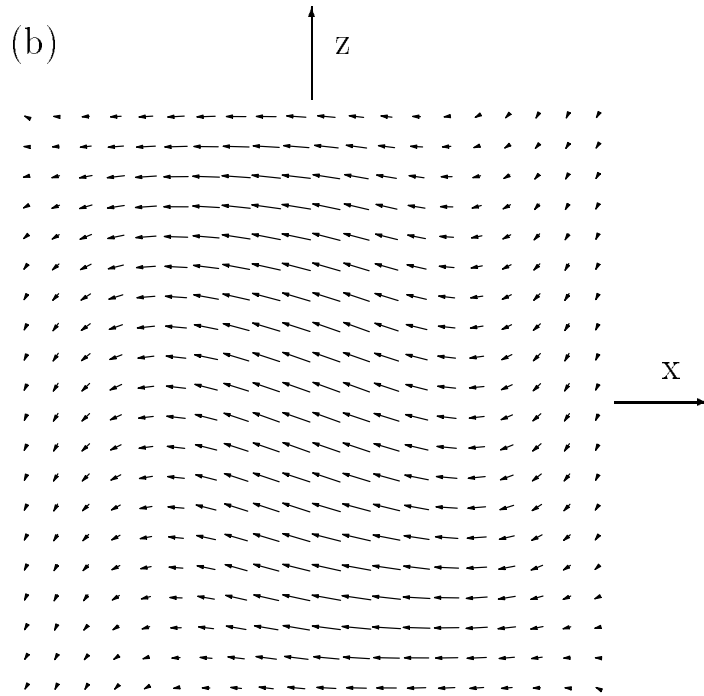
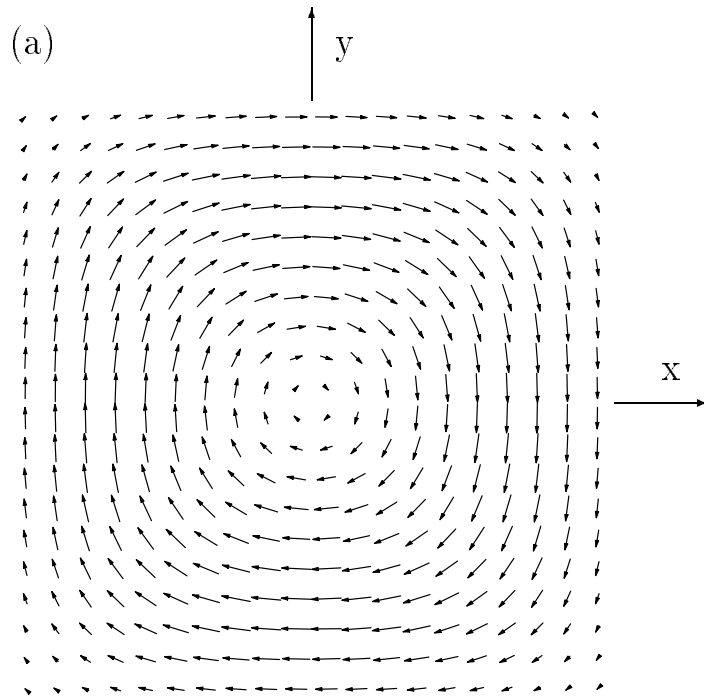


*Fig. 2*



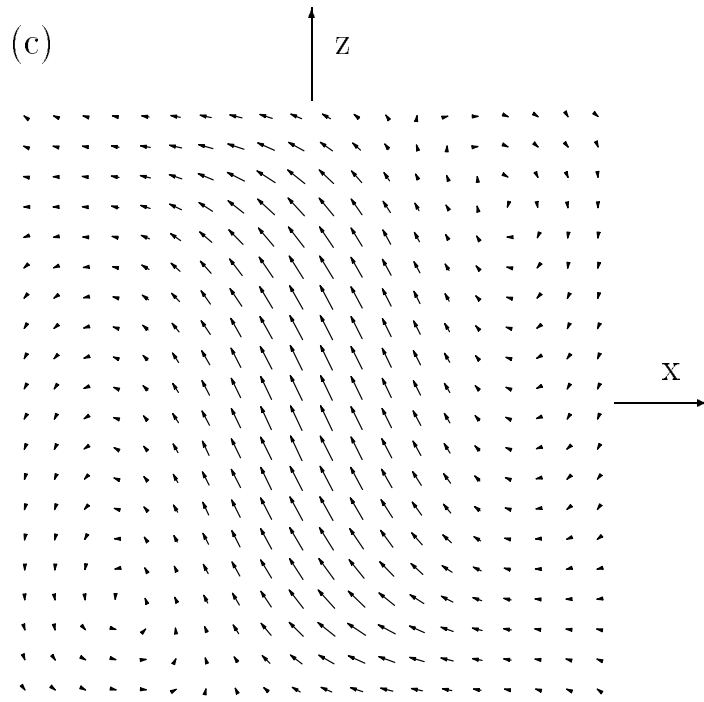


*Fig. 2*



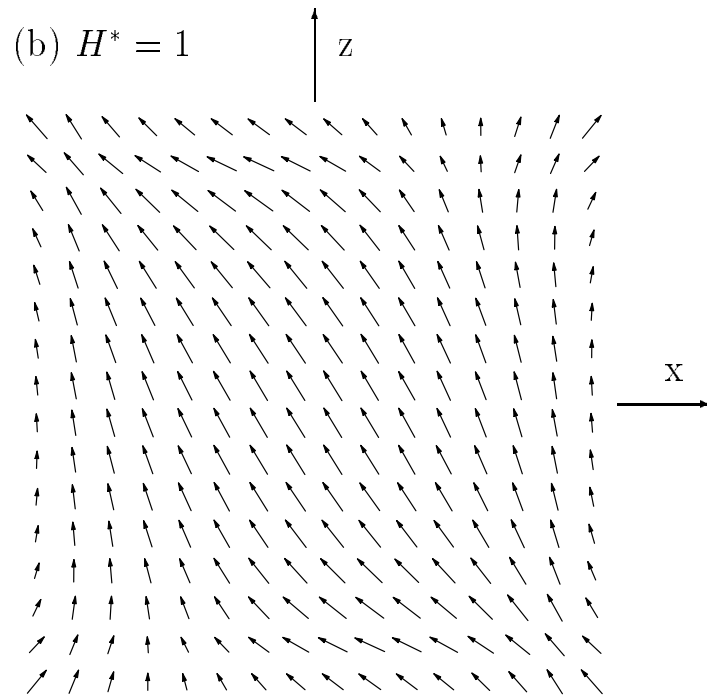
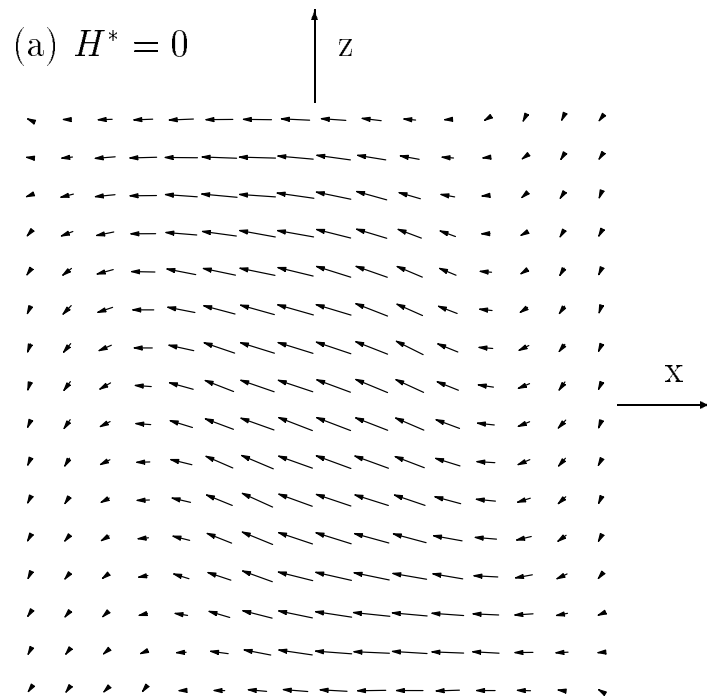
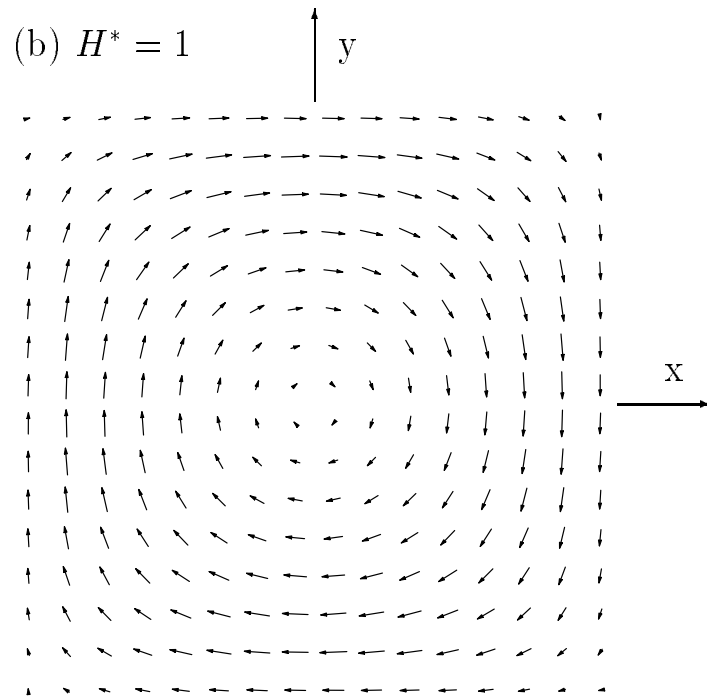
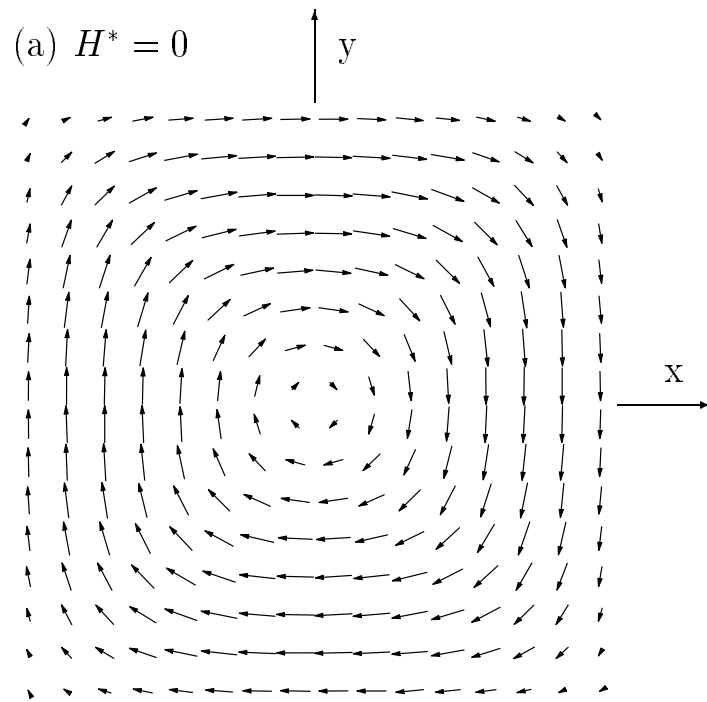
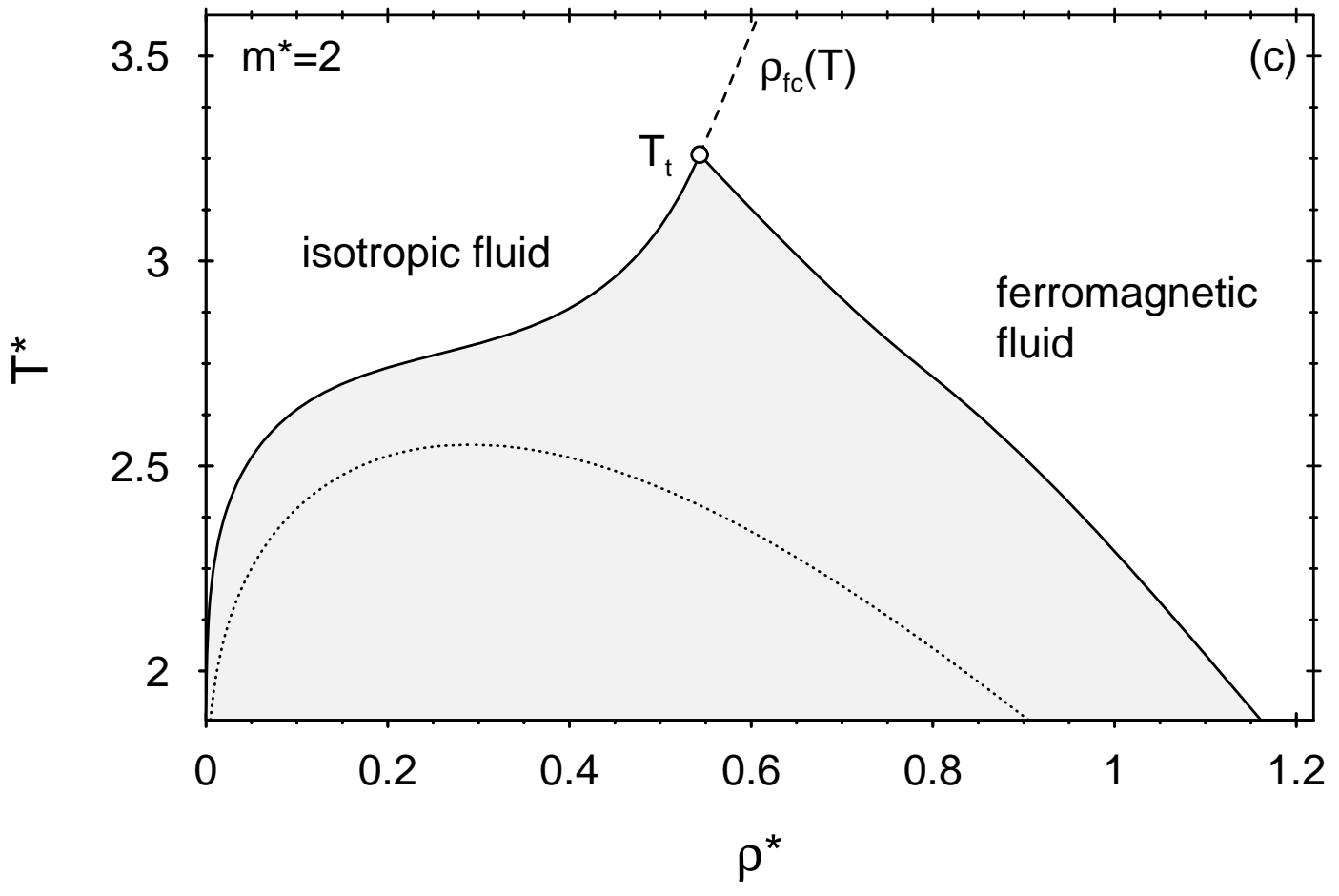


Fig. 6



*Fig. 5*



*Fig. 1(c)*

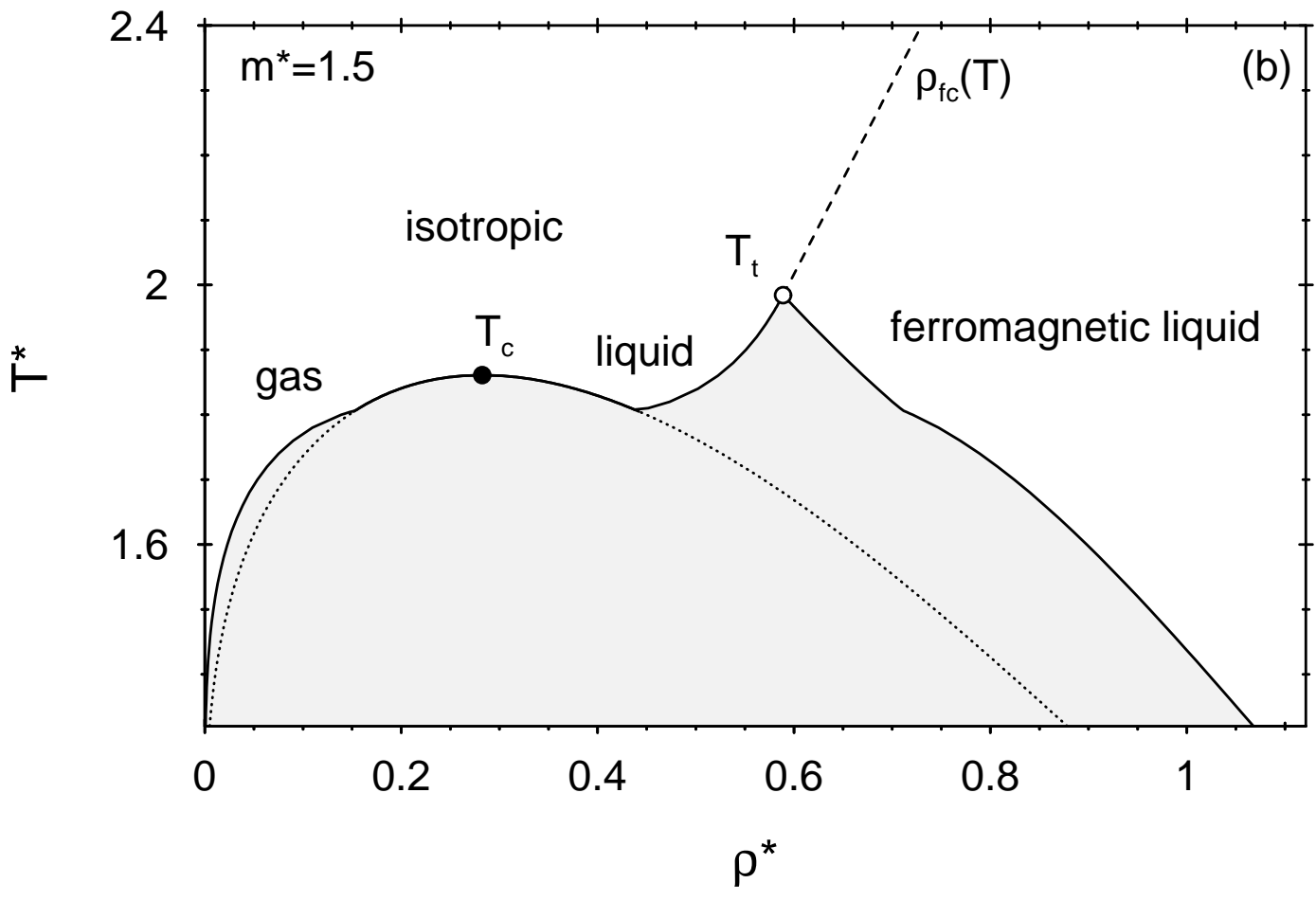


*Fig. 1(b)*

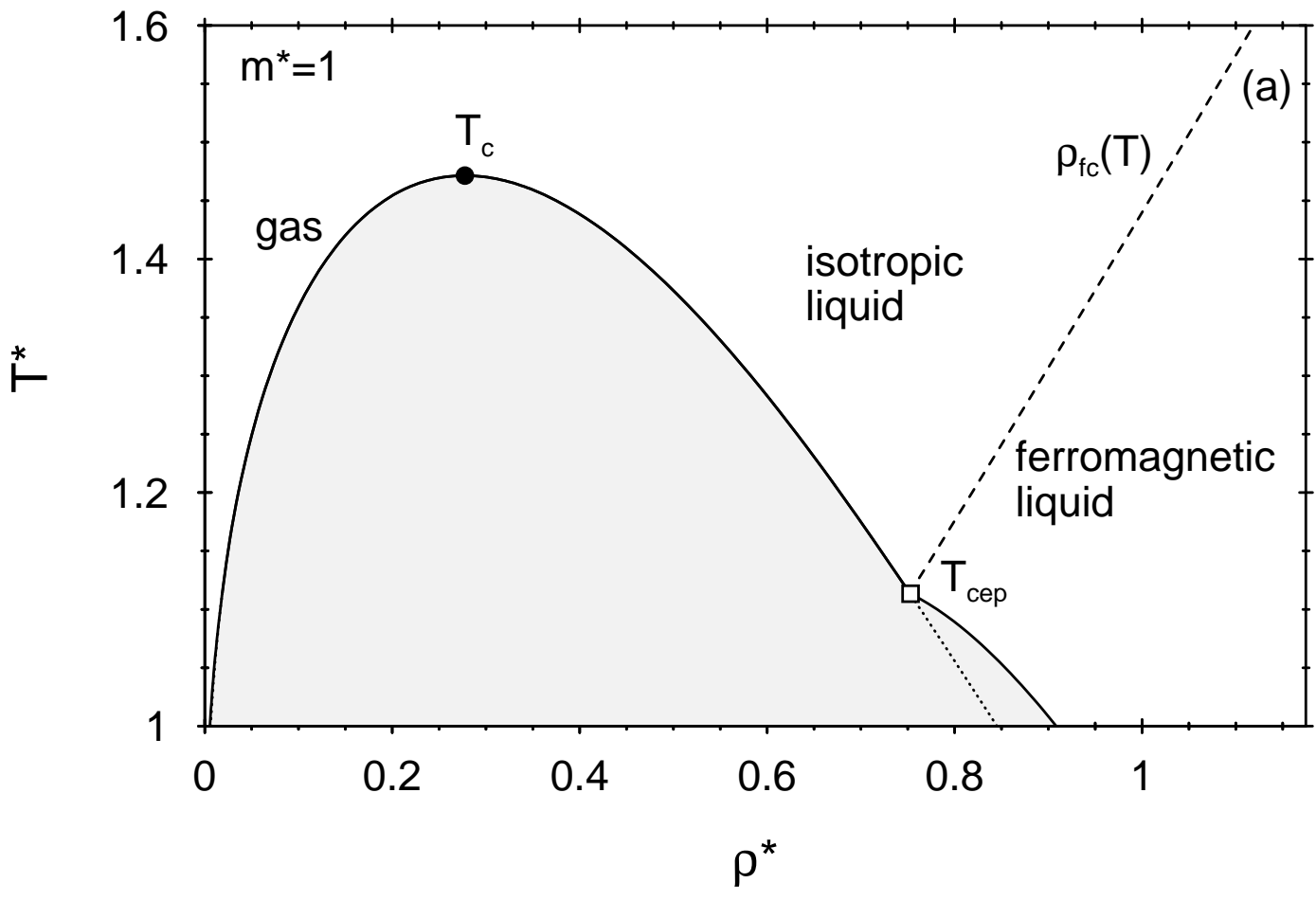


*Fig. 1(a)*

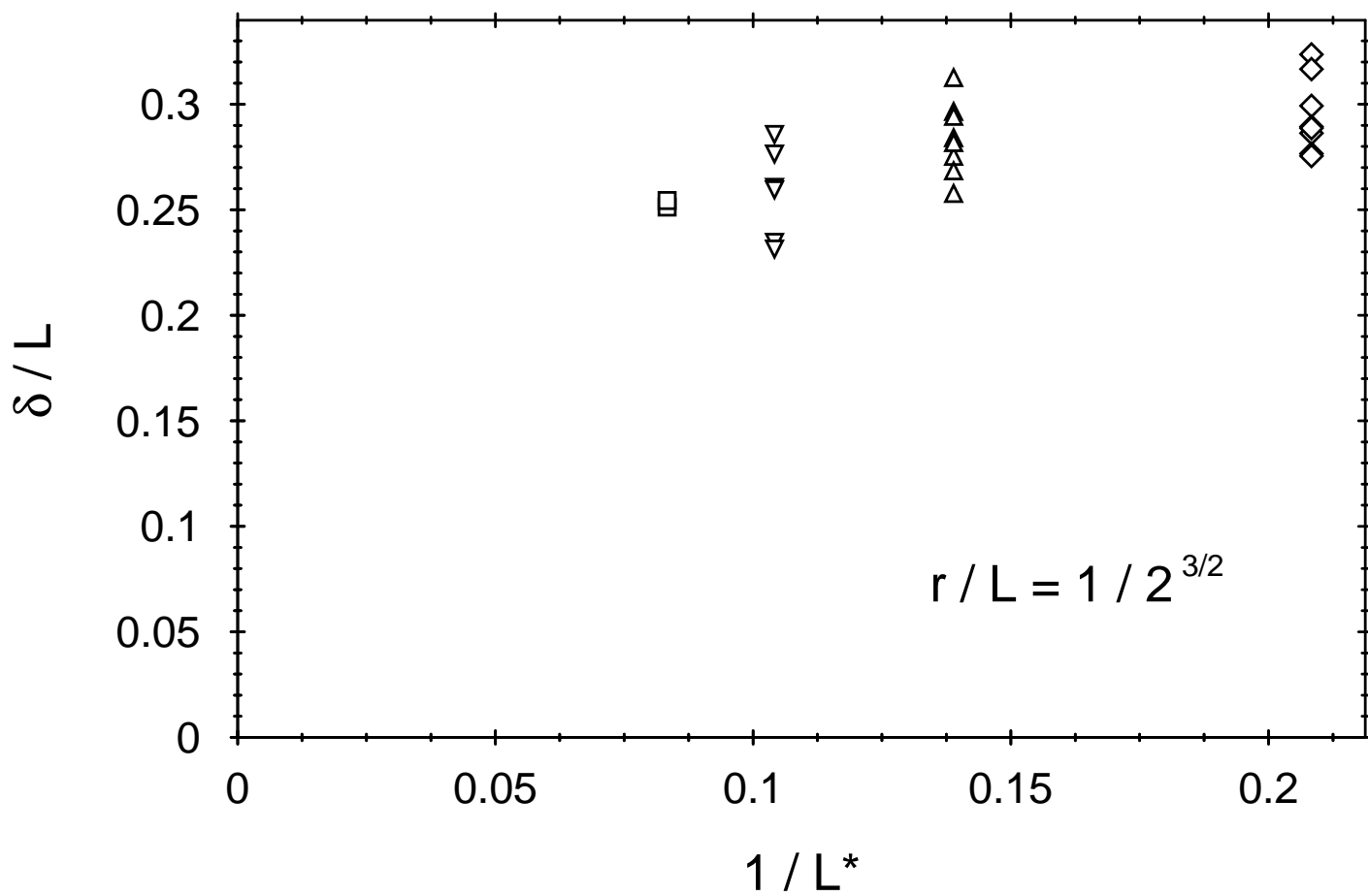


*Fig. 3*

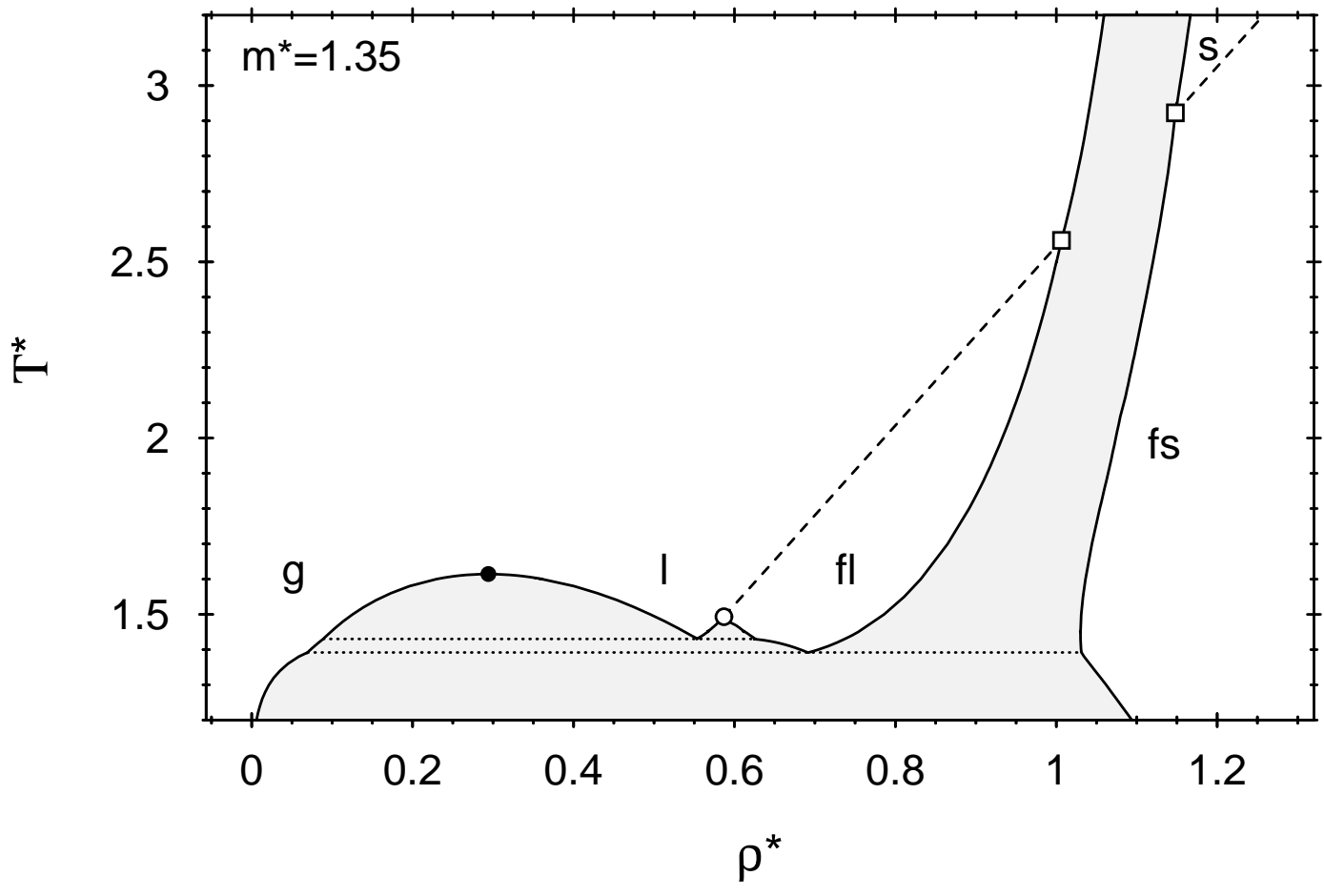


*Fig. 8*

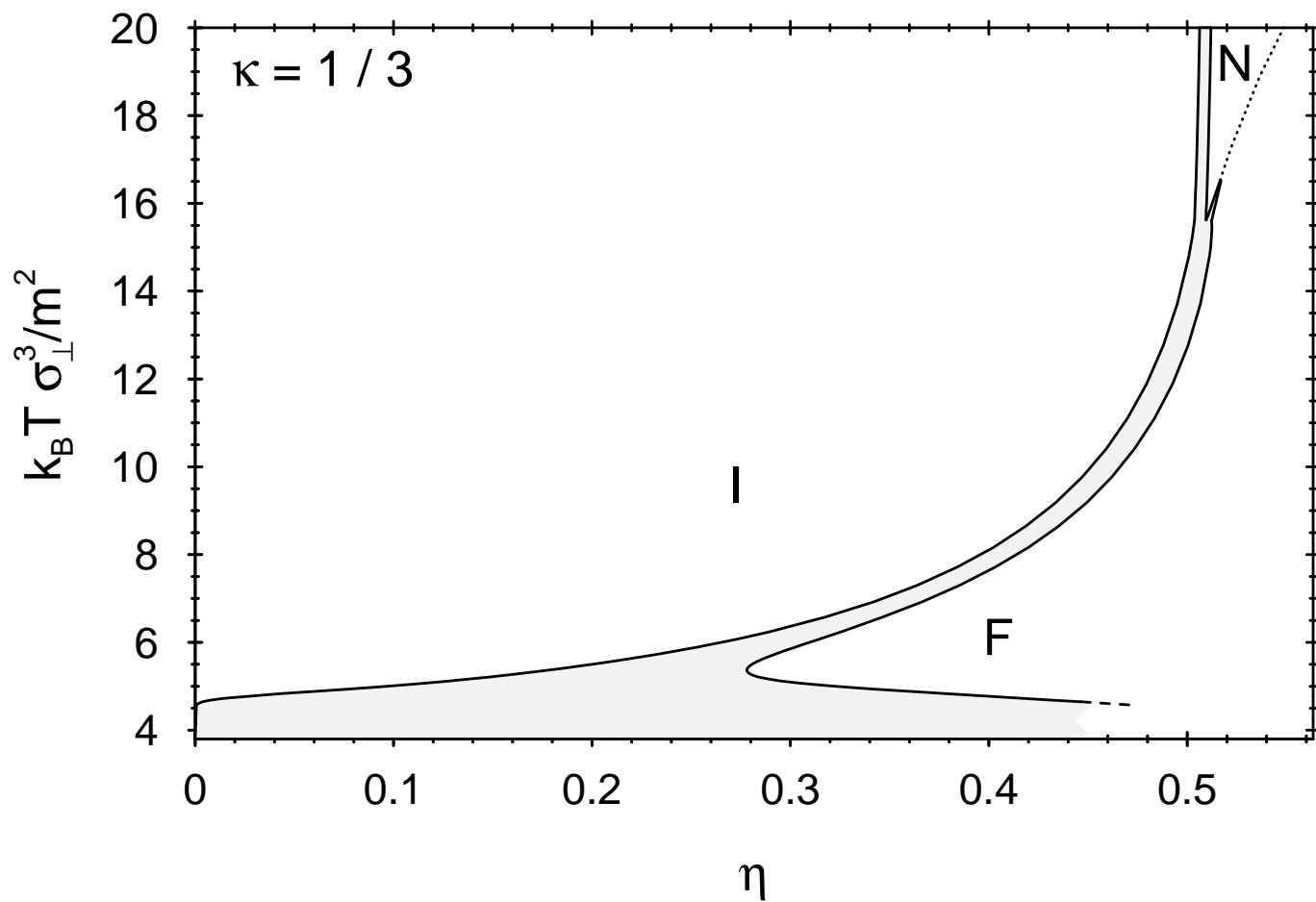


*Fig. 11*



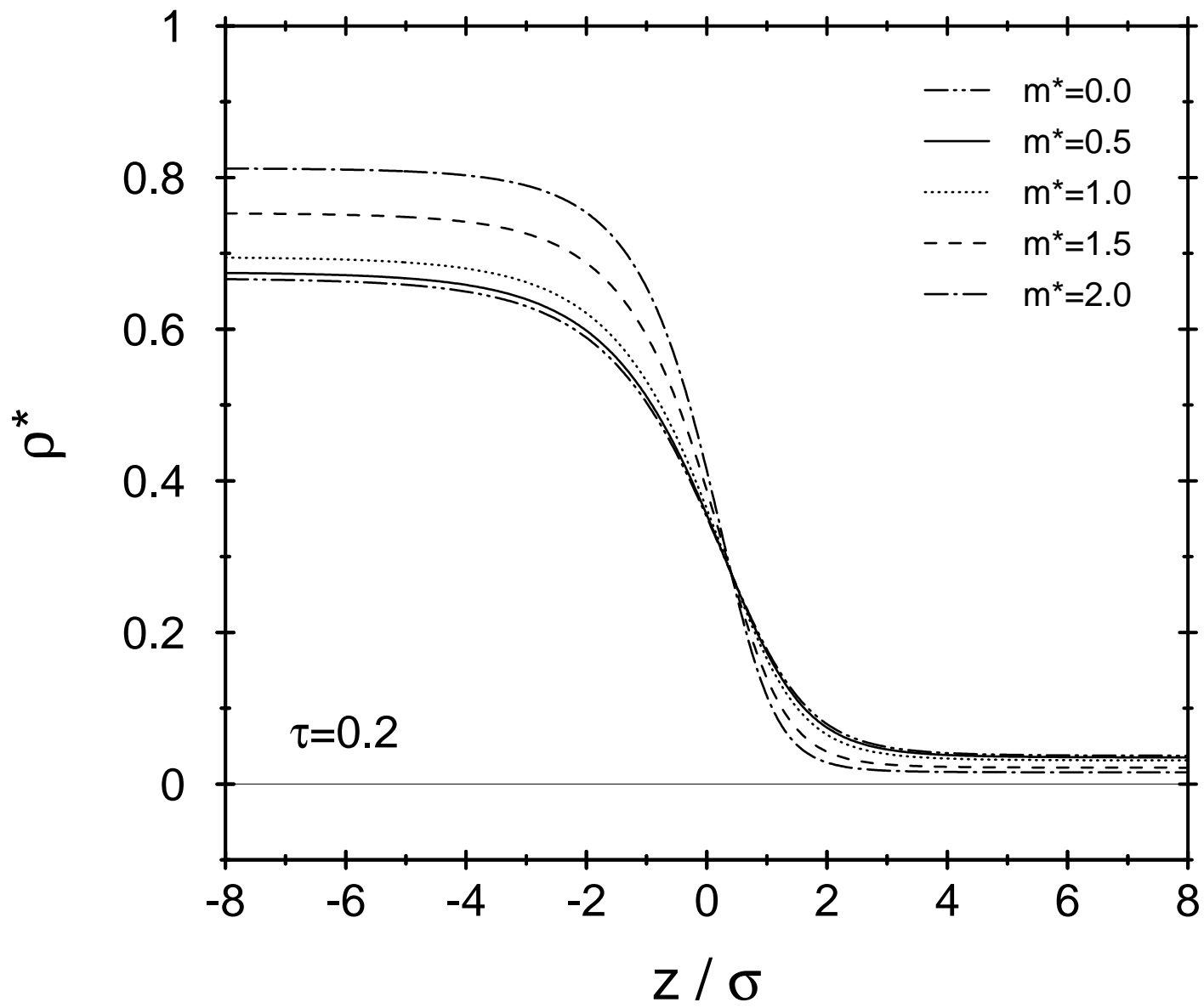


Fig. 12

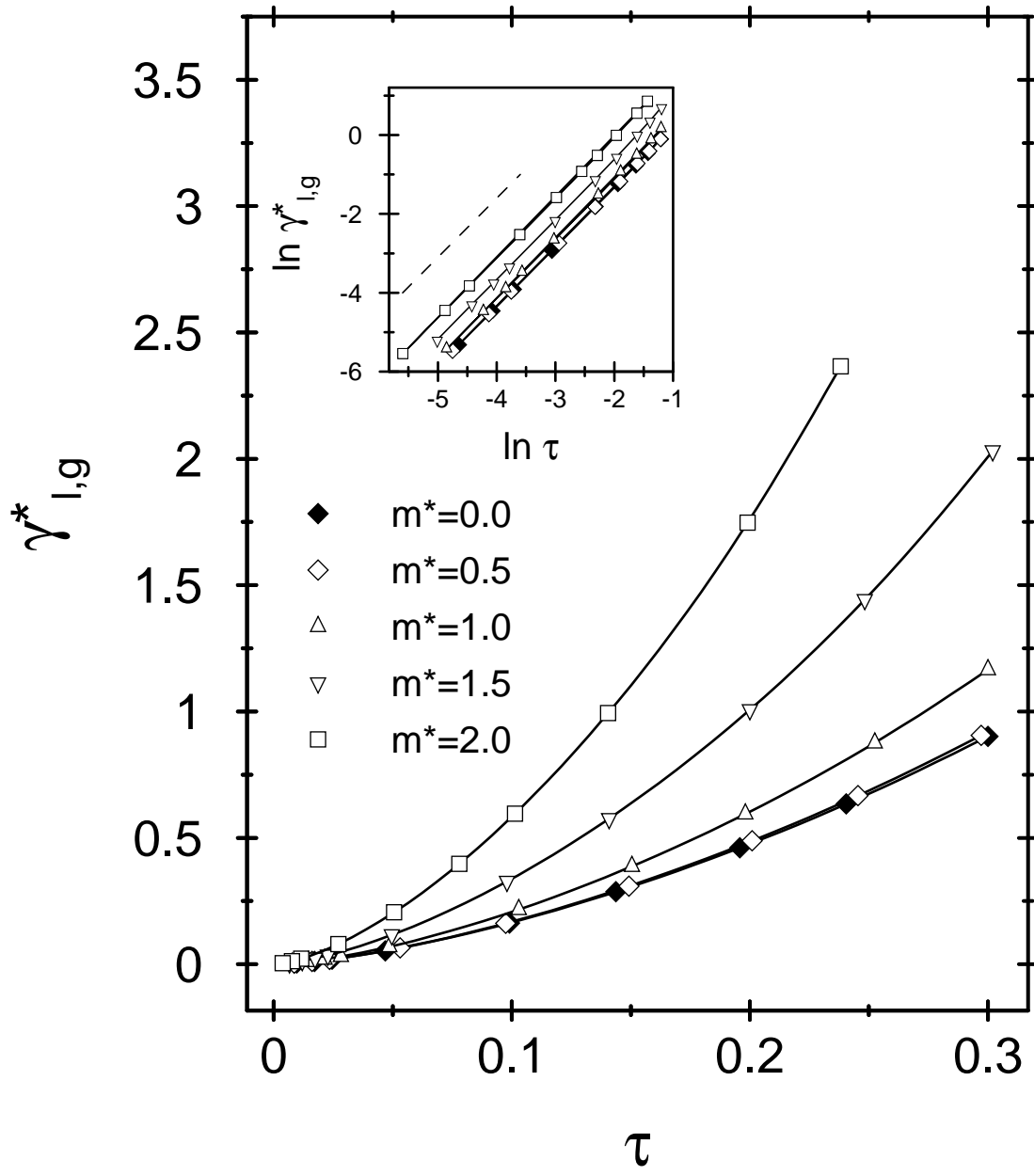


Fig. 14